Late Quaternary fluvial terraces of the Romagna and Marche Apennines, Italy: Climatic, lithologic, and tectonic controls on terrace genesis in an active orogen

Karl W. Wegmann [a,*,1], Frank J. Pazzaglia [b]

[a] Department of Marine, Earth, and Atmospheric Sciences, North Carolina State University, Campus Box 8208, Raleigh, NC 27695-8208, USA
[b] Department of Earth and Environmental Sciences, Lehigh University, Bethlehem, PA 18015, USA

ABSTRACT

We synthesize a new fluvial terrace chronostratigraphy of the Bidente and Musone Rivers cast within a broader European framework, which forms the basis of a terrace genesis and river incision model for the northern Apennines, Italy. Our model, supported by terrace long profiles, correlation to Po foreland sediments, 15 new radiocarbon dates, and published numeric and relative stratigraphic ages, highlights how drainage basin substrate drives concurrent formation of strath terraces in the Bidente basin and fill terraces in the Musone basin. Quaternary climate change paces the formative geomorphic processes through unsteady discharges of water and sediment. In the weathering-limited setting represented by the Bidente basin, siliciclastic detritus carves broad strath surfaces during glacial climates that are preserved as terraces as the river incises during the transition to an interglacial climate. In contrast, the transport-limited and carbonate detritus dominated Musone basin sees valleys deeply buried by aggradation during glacial climates followed by river incision during the transition to an interglacial climate. Incision of these rivers over the past ∼1 million years has been both unsteady and non-uniform. These and all Po-Adriatic draining rivers are proximal to a base level defined by mean sea level and have little room for increasing their longitudinal profile concavities through incision, particularly in their lower reaches despite periodic glacio-eustatic drawdowns. As a result, the observed incision is best explained by rock uplift associated with active local fault or fold growth embedded in the actively thickening and uplifting Apennine foreland.

© 2008 Elsevier Ltd. All rights reserved.

1. Introduction

Excellent preservation, exposures, and a long history of river terrace studies in the central and northern Apennines, Italy are here synthesized into a comprehensive model describing terrace genesis and deformation in response to variable climatic, base level, and lithologic factors. The Apennines offer a favorable setting where the respective contributions of these factors in the development of the modern landscape can be individually assessed. Apennine orogenesis features concurrent and paired belts of crustal short-ening and extension (e.g. Elter et al., 1975) and rapid, recent, regional topographic emergence within the past three million years (Bartolini, 2003). The interaction between a complex geology, characterized by the distribution of carbonate and siliciclastic rocks, and Pleistocene glacial–interglacial climate variability imparts unique hydrogeomorphic responses on adjacent drainage basins, rendering an individual basin's response to tectonic or glacio-eustatic driven base level changes equivocal. For example, terrace studies from northern Apennine basins draining to the Po-Adriatic foreland have been utilized as supporting evidence for steady-state topography (Simoni et al., 2003); gravitational collapse of a tectonically inactive Apennine fold-and-thrust belt (Bertotti et al., 1997); epeirogenic uplift and northeast-to-east oriented tilting of the frontal portion of the northern Apennines accompanied by shallow-crustal extension (Bertotti et al., 1997; Di Bucci et al., 2003; Mariani et al., 2007); anticlinal growth above shallow blind thrust faults (Vannoli et al., 2004); contractional deformation near the mountain front above either a shallow active range-bounding blind (Amorosi et al., 1996) or emergent (Benedetti et al., 2003) thrust fault; or a developing deeply buried crustal ramp (Lavecchia et al., 2003; Pauselli et al., 2006; Picotti and Pazzaglia, 2008). Models stressing epeirogenic processes typically conclude that fault-related folds are embedded in the uplifting landscape but are no longer active (Lavecchia et al., 2003; Mayer et al., 2003; Borraccini et al., 2004).

Lacking in these and related studies is a synoptic view that reconciles existing observations with new data to construct a consistent and broadly applicable model for terrace genesis in the northern and central Apennines for the past 500 ka. Such a model is

* Corresponding author. Tel.: +1 919 515 0380; fax: +1 919 515 7802.
  E-mail address: karl_wegmann@ncsu.edu (K.W. Wegmann).
[1] Formerly at Lehigh University.

the primary goal of this paper as it provides for an interpretation of the active tectonic regime of the northern Apennines, explains the variable fluvial response to basin rock type, and allows us to propose an integrated Quaternary stratigraphic framework, applicable to terrace formation in the Apennines in the context of a large body of work describing the terraces of numerous European rivers.

This study focuses on the Bidente and Musone River basins located in the Romagna and Marche Apennines, respectively (Fig. 1); two drainage systems with contrasting geology, exceptional terrace exposures, and ample opportunities for numeric dating of terrace alluvium. We use river terraces and correlative deposits beneath the Po Plain to develop a terrace chronostratigraphy resulting from Late Quaternary climate unsteadiness. Numeric ages are gathered for terrace straths and used to convert measured strath separation from the channel into a river incision rate. Our arguments are built upon the foundation of numerous excellent fluvial and tectonic geomorphology studies completed in the Apennines and elsewhere. Our results highlight similarities and differences in the incision histories of the Bidente and Musone Rivers consistent with an interpretation of continued shortening across the foreland flank of the northern Apennines and rock uplift

that has been unsteady. In addition, non-uniform incision suggests that deformation is localized, indicating the presence of faults or growing folds.

2. Tectonic setting of the northern Apennines

The Apennines are a Tertiary fold-and-thrust belt defining part of the plate boundary between Europe and Africa (Adria) (McKenzie, 1972). Peninsular Italy is the result of Oligocene-to-recent growth of the Apennine orogenic wedge driven by Adria (e.g. Grenerczy et al., 2005) subduction and upper plate counter-clockwise rotation about an Euler pole located in the western Alps (Reutter, 1981; Patacca et al., 1990; Pini, 1999). The subduction zone has undergone significant rollback to the east–southeast resulting in an Apennine orogenic wedge marked by a paired contractional leading edge and extensional trailing edge (e.g. Elter et al., 1975; Malinverno and Ryan, 1986; Royden, 1993; Cavinato and DeCelles, 1999; Wortel and Spakman, 2000).

From 30 to 4 Ma the Apennine wedge remained submerged as it overrode thinned deep-water continental lithosphere capped predominantly by Tethyan carbonates. The wedge grew by
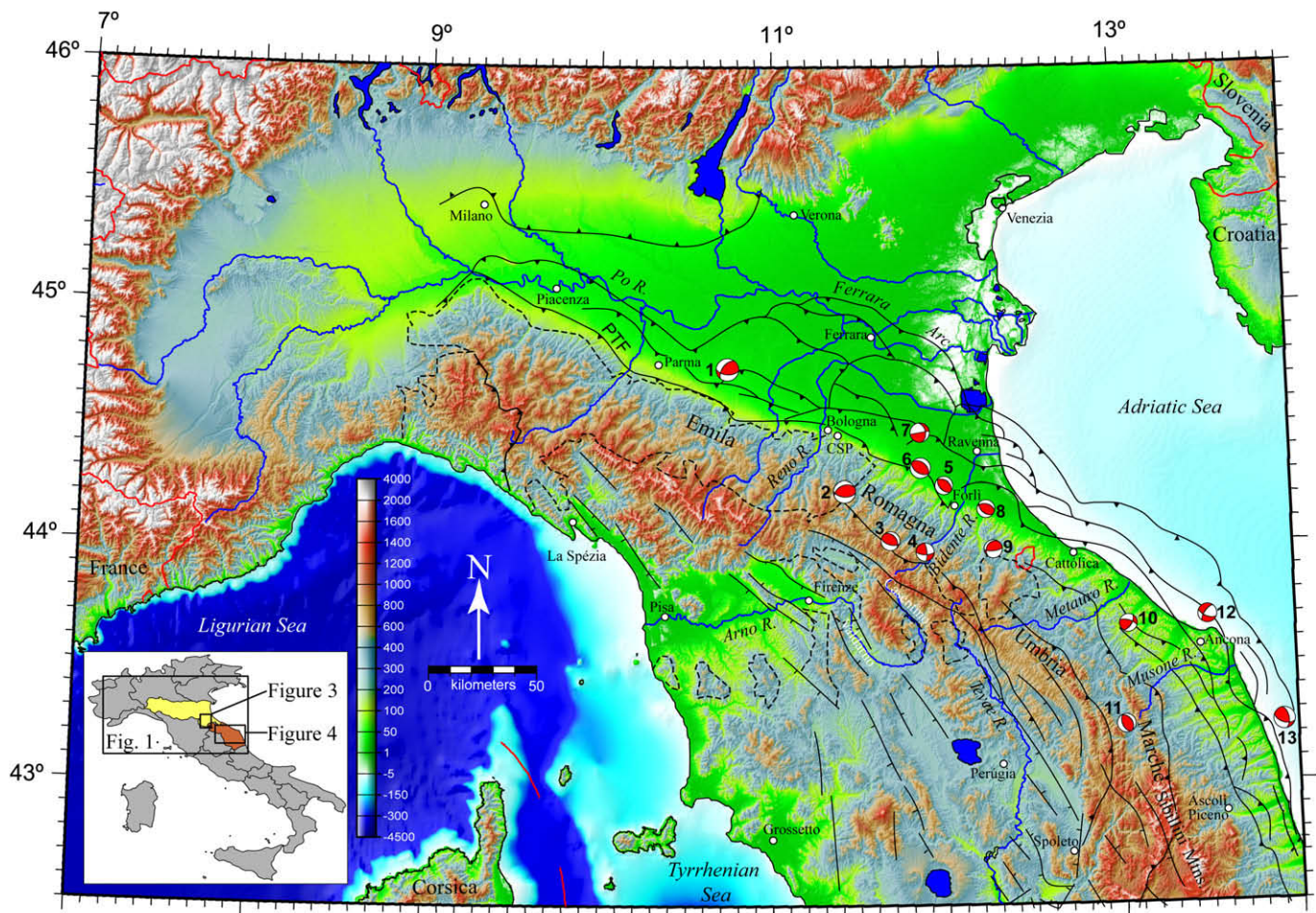
Fig. 1. Topography of the Northern Apennines derived from 90-m SRTM digital elevation model. Key regions and drainage systems are labeled. Thrust and normal faults are shown with symbols on the hanging wall. Dashed-line polygons denote outcroppings of the Ligurian Nappe. The lower left inset shows the location of Figs. 1,3 and 4. The Emilia–Romagna and Marche regions are shown in yellow and brown, respectively. CSP, Castel San Pietro, where Cyr and Granger (2008) report cosmogenic burial ages for Imola Sands "Sabbie Gialle" (IMO 1) deposits. PTF, Pedeapenninic thrust fault according to Boccaletti et al. (2004). Selected earthquake focal mechanisms are shown with compressional quadrants colored and numbers adjacent to focal mechanisms identify specific earthquakes as to their magnitude (Mw), depth (km), and regional centroid moment tensor event ID as follows. (1) $M = 5.4$, $Z = 15$, ID = B101596C; (2) $M = 5.3$, $Z = 23$, ID = R091403A; (3) $M = 4.6$, $Z = 29$, ID = R041606A; (4) $M = 4.4$, $Z = 35$, ID = R012599B; (5) $M = 4.3$, $Z = 22$, ID = R050200A; (6) $M = 4.9$, $Z = 21$, ID = R051000A; (7) $M = 4.7$, $Z = 15$, ID = S120578A; (8) $M = 4.3$, $Z = 17$, ID = R120703A; (9) $M = 4.4$, $Z = 19$, ID = R080100A; (10) $M = 4.3$, $Z = 42$, ID = R102106A; (11) $M = 4.5$, $Z = 41$, ID = R090200A; (12) $M = 5.1$, $Z = 15$, ID = S070387A; (13) $M = 4.5$, $Z = 25$, ID = n/a. Earthquake sources are Pondrelli et al. (2006), Gasparini et al. (1985), and from the online Quick RCMT catalog: http://mednet.rm.ingv.it/quick_rcmt.php [accessed 11.04.07].

underplating of these Adrian crustal rocks, olistostromes and sili-ciclastic turbidites deposited in a series of foredeep basins developed successively in front of the advancing wedge (the Late Oligocene to Late Miocene Macigno, Cervarola, Marnoso Arenacea, and Laga basins; Ricci Lucchi, 1986). These foredeeps are now in the footwall of the Ligurian nappe, a large, contiguous structural lid of the orogenic wedge comprising Jurassic–Eocene ophiolite and sedimentary rocks of an older, Alpine accretionary complex rifted away from Europe during original rollback (Boccaletti et al., 1971; Kligfield, 1979; Feroni et al., 2001).

The wedge, including the Ligurian nappe, emerged above sea level by about 4 Ma as it advanced over the thicker west-facing passive margin of the Adriatic continental platform. Topographic relief and initiation of an Apennine mountain front grew with emergence of the wedge during the Late Pliocene to Early Pleistocene (Castellarin et al., 1985; Bartolini, 2003; Picotti and Pazzaglia, 2008). The ~4 km thick Ligurian nappe has been unroofed from the Romagna and Marche Apennines, presumably by erosion since the Late Pliocene (Zattin et al., 2000; Feroni et al., 2001) (Fig. 1).

Two groups of geodynamic models have been proposed to account for Quaternary uplift, deformation, and topographic growth of the northern Apennines. One group appeals to regional, late stage epeirogeny and local gravitational collapse of an otherwise tectonically *inactive* fold-and-thrust belt (Bertotti et al., 1997; Coltorti and Pieruccini, 1997, 1999; Calamita et al., 1999; Carminati et al., 1999; D'Agostino et al., 2001; Di Bucci and Mazzoli, 2002; Argnani et al., 2003; Di Bucci et al., 2003), perhaps resulting from asthenospheric diapirism (e.g. Wezel, 1982; Bell et al., 2006) and/or a tear in the subducting Adriatic slab (e.g. Wortel and Spakman, 2000; Scrocca, 2006). The other group advocates for an *active* and *dynamic* Apennine orogenic wedge where deformation is the response to ongoing rollback of Adria, driving shortening in the Po-Adriatic foreland and extension in the Tyrrhenian backarc (Bartole, 1995; Montone and Mariucci, 1999; Montone et al., 1999, 2004; Picotti and Pazzaglia, 2008). Active seismicity in the foreland is both deep and compressional (15–40 km), arguing for whole crustal involvement in the shortening (e.g. Lavecchia et al., 2003; Pondrelli et al., 2006) (Fig. 1).

3. Geologic and geomorphic setting of the Bidente and Musone basins

We focus on the Bidente and Musone River basins in order to compare the along-strike differences in incision rate for parts of the Apennine front that share similar positions near the center of arcuate thrust sheets but differ in their base level and underlying rock types (Fig. 2). The Bidente basin drains the northeastern flank of the Apennines, heading at the drainage divide between Toscana and Romagna and intersecting the southern margin of the Po Plain just south of Forli. It continues onto the Po Plain (as the Ronco River following its confluence with the Voltare River) and enters the Adriatic Sea at Ravenna (Figs. 1 and 3). The drainage basin covers ~475 km^2 upstream of its intersection with the Po Plain. Basin elevations decrease from 1650 m along the Tuscan divide to 40 m at the Po Plain. The Bidente valley contains only strath terraces and the channel is carved into bedrock at the mountain front (Fig. 3). Middle-to-Late Pleistocene glacio-eustatic drawdowns are known not to have reached Forli as headward-migrating knickpoints (Amorosi et al., 2004); rather, the Bidente built large lowstand progradational fans north onto the Po Plain during sea level lowstands (e.g. Di Dio, 1998; Amorosi et al., 2004).

Much of the Romagna Apennines are an erosional window though the Ligurian nappe exposing a more or less uniform distribution of Miocene siliciclastic trench turbidites of the Marnoso Arenacea Fm (Pini, 1999; Feroni et al., 2001) (Fig. 2A) across the upper three quarters of the drainage basin. This sandstone accounts for the majority of the pebble to boulder-sized bedload of the channel. Rock mass strength of the Marnoso Arenacea Fm increases towards the southern drainage divide in step with increases in the maximum depth of burial (Ricci Lucchi, 1986; Zattin et al., 2000). In contrast, the downstream quarter of the basin is underlain by a homoclinally dipping sequence of upper Miocene (Messinian Colombacci Fm) through Pliocene (Argille Azurre Fm) marine silt and mudstones with local tabular sandstone interbeds (Lipparini et al., 1968; Amorosi et al., 1998a) (Fig. 2A). Although wide straths are formed on top of these deposits, which are particularly susceptible to channel and valley widening, they do not represent a large fraction of the bedload of either the modern river or as clasts in strath terrace deposits. Bedrock is exposed along channel trunks and in numerous landslide scars. Hillslopes are otherwise mantled by ~1 m of colluvium. The modern Bidente channel is predominately bedrock-floored upstream of Santa Sofia, an under-capacity, mixed bedrock-alluvial channel downstream, and everywhere flows within broad incised meanders set into a Late Pleistocene valley (Fig. 3).

The orientation of the Bidente valley is parallel to the orogenic slope and perpendicular to the dominant structural grain (Fig. 2A). The channel crosses several major orogen parallel NW–SE oriented thrust faults and related folds within the Marnoso Arenacea Fm (Pignone et al., 1994, 2001). Drainage basin relief is strongly influenced by these Tertiary faults and folds as well as the outcropping of individual thick, resistant beds, which impart an overall NW–SE linearity to the topography (Fig. 3).

The central Marche Apennines are dominated by NW–SE trending asymmetric folds detached from the underlying basement along Triassic anhydrates (De Feyter et al., 1986). Similar in structural style to the Romagna Apennines, these fault-cored folds expose deeper structural levels, bringing Mesozoic and lower Tertiary carbonates (Centamore et al., 1991) to the surface where they form prominent topographic ridges, known from west to east as the Umbria–Marche, Marche, Cingoli, and Monte Conero anticlines (Figs. 2B and 4). The Marche anticlinal ridges culminate in peaks with elevations from ~1500 m in the north to 2400 m in the Sibillini Mountains to the south (Fig. 4). All of the major rivers of central Marche cut across one or more of these anticlinal ridges in deep gorges (Fig. 4). The Musone River drains eastward from its headwaters on the 1450-m high Marche ridge, exploits strike valleys, and then cuts across the Cingoli ridge in a 300-m deep gorge en route to the Adriatic Sea south of Ancona (Figs. 1 and 4). The Cingoli Gorge is carved through the Late Cretaceous–Eocene Scaglia formations and is cored by the Cingoli ramp anticline (Nanni, 1996). After exiting Cingoli Gorge, the river traverses soft Mio-Pliocene hemipelagic and turbiditic foredeep rocks and then a broadly folded and faulted succession of lower Pliocene-to-Pleistocene shallow marine pelitic wedge-top basin deposits (Fig. 2B; Bigi et al., 1997; Pauselli et al., 2006). The shortening responsible for anticline growth began in the Early Miocene and propagated to the northeast. The most external thrust front is beneath the Adriatic Sea, east of Ancona (Fig. 1). Thick calcareous colluvium ($\geq$10 m) derived from physical weathering of the carbonate ridges typically mantles lower slopes of the anticlinal ridges and interfinger with fluvially transported sediments.

The lower 35 km of the Musone channel is completely alluvial, but near the town of Filotrano the Musone valley and channel is incised into soft Middle Pliocene–Early Pleistocene marine mudstone (Fig. 2B). The Musone remains a bedrock-to-mixed bedrock channel for 12 km through this reach, until 2 km past San Vittore, where it transitions back to an alluvial channel for 5 km until intersecting the mouth of Cingoli Gorge. As with the Bidente, the Musone generally flows parallel to the orogenic slope and perpendicular to major structural features (Figs. 2 and 4).
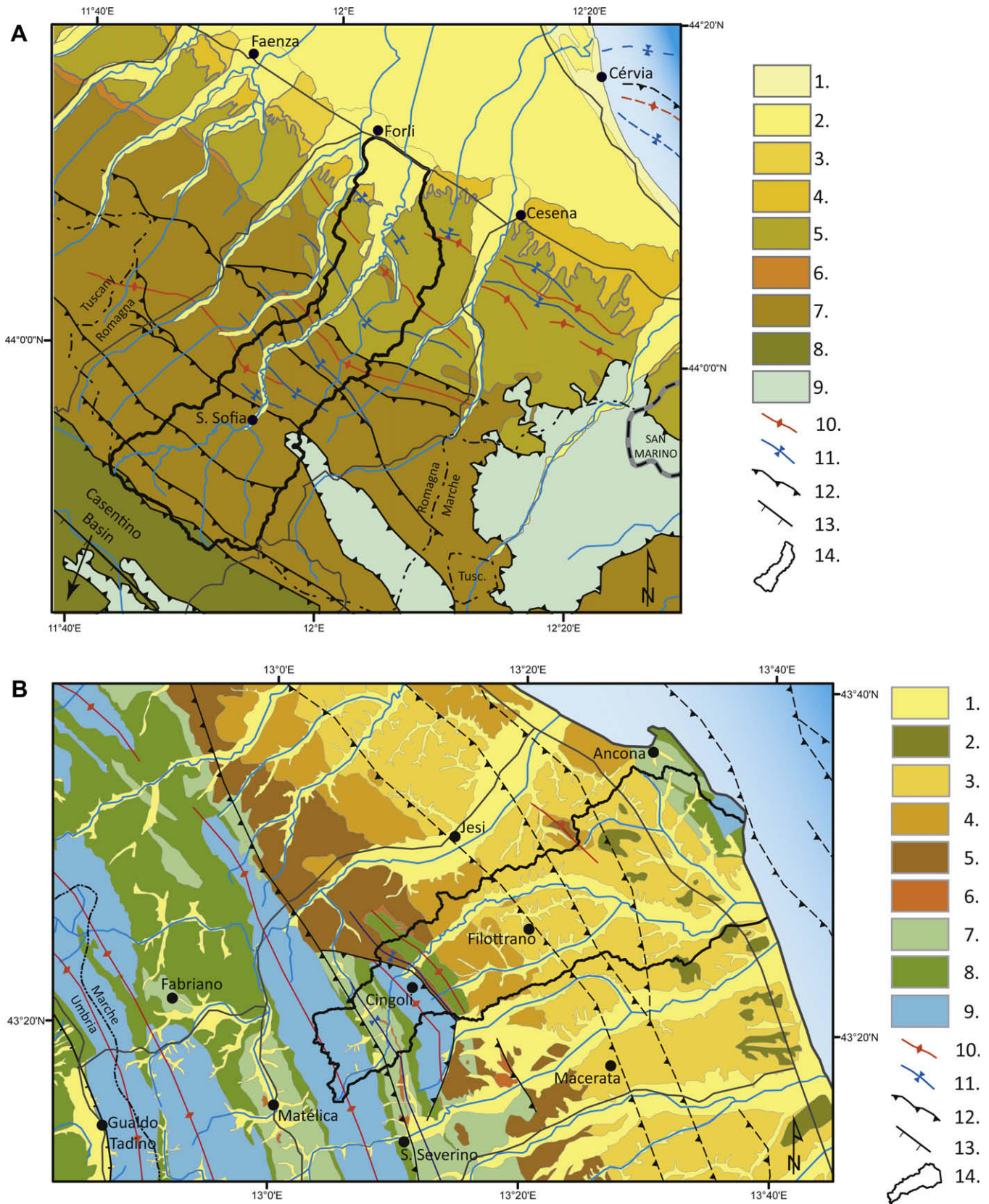
Fig. 2. Simplified Geologic maps of A. Romagna and B. Marche Apennines at 1:400,000-scale, modified from 1:100,000-scale Carta Geologica D'Italia maps – Foglios 99, 100, 107, 108, 116–118, and 123–125 (Agenzia per la protezione dell'ambiente e per i servizi tecnici, 2007). Romagna map legend: 1. Holocene beach and dunes; 2. Late Pleistocene-to-Holocene alluvium and terraces; 3. Early Middle Pleistocene alluvial to shallow marine; 4. Late Pliocene to Early Pleistocene shallow marine; 5. Messinian to Pliocene marine; 6. Messinian evaporites; 7. Middle Miocene Marnoso Arenacea Fm; 8. Late Oligocene to Early Miocene marine Macigno Fm; 9. Eocene to Upper Cretaceous Ligurian Nappes; 10. Anticline, dashed where inferred; 11. Syncline, dashed where inferred; 12. Thrust fault, teeth on upthrown side, dashed where inferred; 13. Normal fault, teeth on down-thrown side; 14. Bidente River basin. Marche map legend: 1. Pleistocene-to-Holocene alluvium; 2. Early Middle Pleistocene beach deposits, possible lateral equivalents to the Imola sands (Sabbie Gialle); 3. Upper Pliocene to lower Pleistocene marine; 4. Middle Pliocene marine; 5. Lower Pliocene marine; 6. Messinian evaporites; 7. Messinian marine; 8. Middle Miocene Schlier Formation; 9. Cretaceous to Early Tertiary carbonates; 10. Anticline, dashed where inferred; 11. Syncline, dashed where inferred; 12. Thrust fault, teeth on upthrown side; 13. Normal fault, teeth on the down-thrown side; 14. Musone River basin.
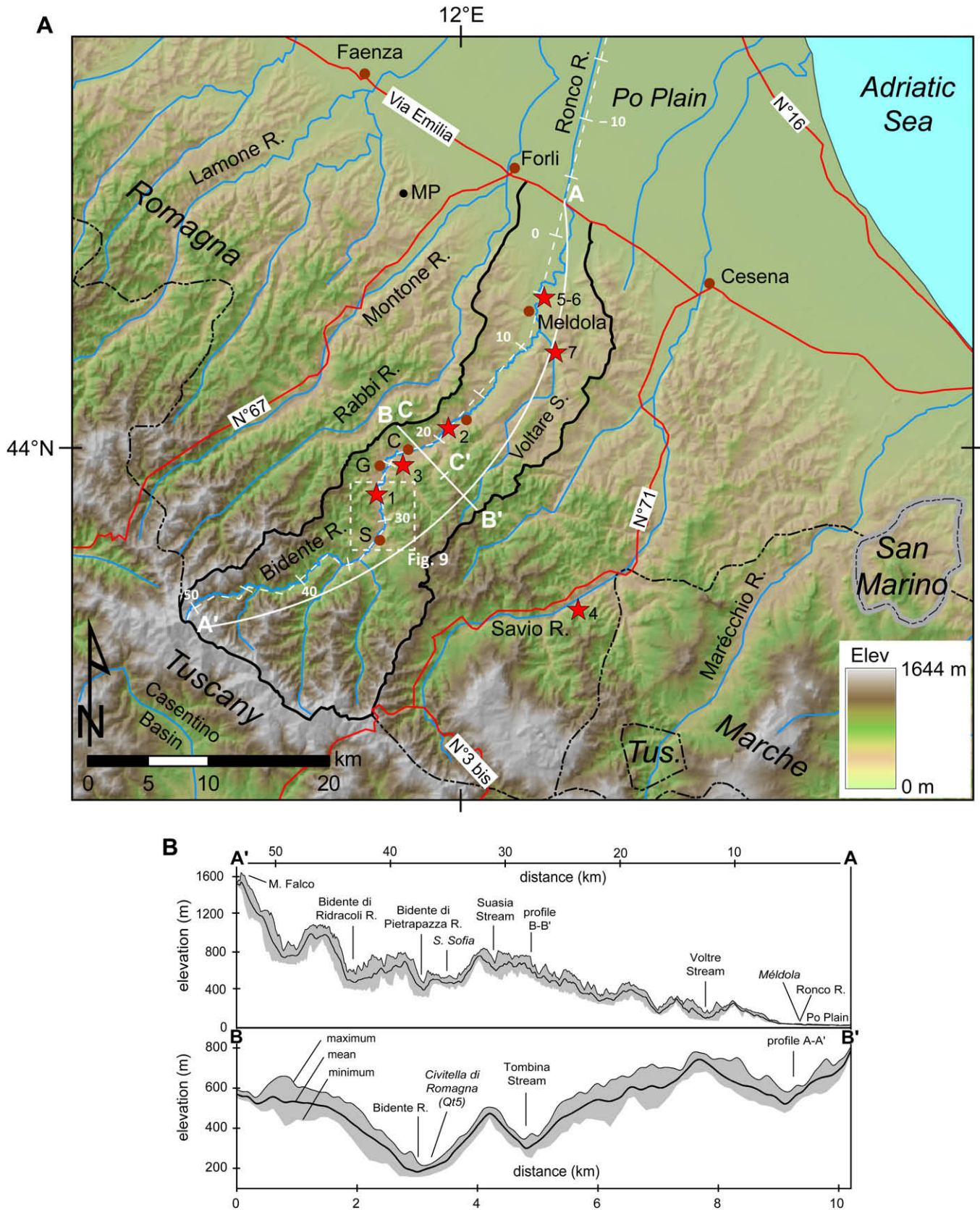
Fig. 3. A. Digital shaded relief map of eastern Romagna outlining the Bidente River basin. Radiocarbon sample locations (red stars and numbers) correspond to Table 1. The modern channel and terrace elevation data are projected to the valley longitudinal profile (dashed white line) that is subdivided into 10 km increments with a zero point at the mountain front. The line of section C–C′ is on Fig. 6. Fig. 9 encompasses the area within the white dashed-line white box. Locations mentioned in the text: C = Civitella di Romagna, G = Galeata, MP = Monte Poggiolo archeological site, N = Nespoli, and S = Santa Sofia. B. Swath topographic profiles of maximum, mean and minimum elevations parallel (A–A′) and orthogonal (B–B′) to the Bidente valley axis.
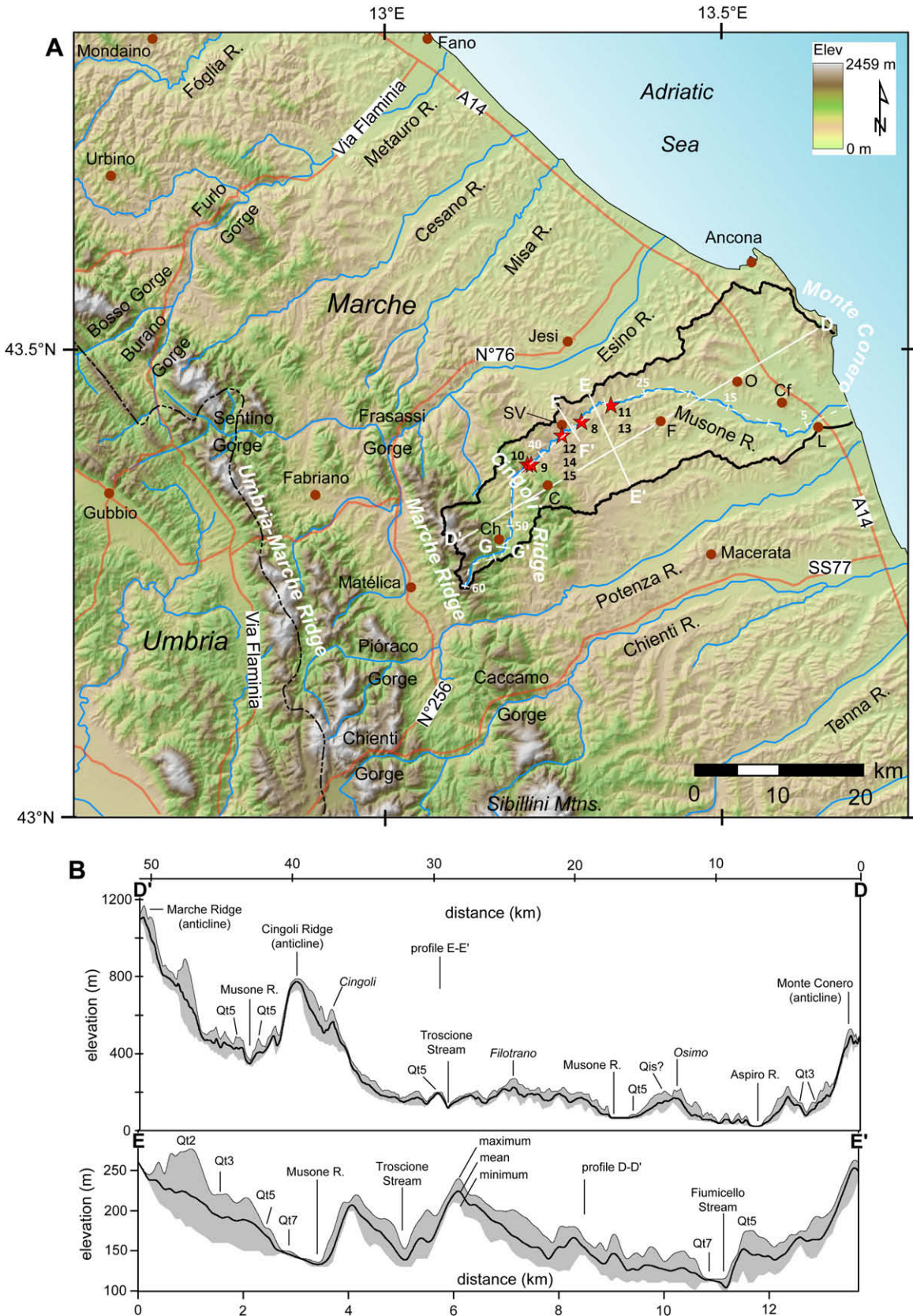
Fig. 4. A. Digital shaded relief map of the northern and central Marche outlining the Musone basin. Radiocarbon sample locations (red stars and numbers) correspond to Table 2. Note the river gorges cut orthogonally across anticlinal ridges (e.g. Cingoli, Marche, and Umbria-March Ridges) that are cored by Mesozoic carbonates. The modern channel and terrace elevation data are projected to the valley longitudinal profile (dashed white line) that is subdivided into 10 km increments. Lines of section F–F′ and G–G′ are shown on Fig. 10. Locations mentioned in the text: C = Cingoli, Cf = Castelfidardo, Ch = Chigiano, F = Filotrano, L = Loreto, O = Osimo, SV = San Vittore. B. Swath topographic profiles of maximum, mean and minimum elevations parallel (D–D′) and orthogonal (E–E′) to the Musone valley axis.

4. Approach and methods for using terraces to measure river incision

River terraces are commonly used to measure the rate of vertical stream incision, typically interpreted as the rate of base level fall, inclusive of rock uplift and associated crustal deformation. An unintended and unfortunate consequence of the availability of high resolution topographic and remote-sensed data has resulted in a focus shift towards using terraces as landforms only, thus effectively disconnecting landform interpretations from key sedimentologic, stratigraphic and numeric age data associated with the terrace deposit. Tectonic interpretations assembled from terrace tread (top) data alone (e.g. Vannoli et al., 2004) are susceptible to problems that we highlight and are able to avoid in the favorable setting of the northern Apennines.

4.1. Terrace straths vs treads as tectonic indicators

River terraces are the geomorphic and sedimentologic expression of unsteady vertical channel incision (e.g. Schumm et al., 1987; Bridgland, 2000). Terrace deposits are unconsolidated allostratigraphic units with a basal unconformity called a "strath" typically cut across bedrock and a constructional bench-like top called a "tread" (Fig. 5A). The deposit can vary vertically and longitudinally in texture, stratification, and thickness. When it is thin (<3 m), it represents the mobile alluvial cover of a bedrock channel (Pazzaglia and Brandon, 2001) and the landform is correctly called a "strath terrace" (Bucher, 1932; Bull, 1991) (Fig. 5B and C). The initial gradient of the strath is the gradient of the channel that cut it, approximated in most cases by the modern channel gradient so

long as the modern channel has a thin mobile alluvial bed in contact with bedrock. In contrast, thick alluvial deposits represent periods of valley aggradation when the channel is vertically raised above its strath; where these thick fills underlie the terrace landform, they are termed "fill terraces" (Bull, 1991) (Fig. 5B and D). In both cases, knowing where the strath lies in the landscape, when it was carved, and when it was abandoned by incision to form the base of a terrace are the pertinent observations leading to a useful terrace genesis model, particularly one that is portable to tectonic problems.

Attempting to utilize terrace treads in a similar way requires caution. The depositional slope of the tread does not always mimic the slope of the underlying strath. Treads are also commonly modified by post-depositional colluvial and tributary alluvial fan burial or fluvial dissection that cumulatively increase their modifications with terrace age (Eppes et al., 2008). In coastal regions, the treads of fan deltas associated with progradational coastlines may have gradients much steeper and of a different slope aspect with respect to the underlying strath. Rivers with high sediment yields that discharge onto low-gradient marine shelves, such as the Marche region of the Adriatic, tend to advance seaward by developing prograding fan deltas during eustatic lows, rather than incising lowstand valleys across the exposed shelf (Thackray, 1998; Woolfe et al., 1998; Pazzaglia and Brandon, 2001). Interpreted neotectonic warping of progradational coastal terraces could very well be relief on the treads of these constructional fan deltas (c.f. Vannoli et al., 2004; Ferranti et al., 2006). Lastly, multiple terrace treads could cap a single terrace deposit and share a common strath. These "fill-cut terraces" say more about complex responses of fluvial processes than they do about rock uplift driven incision (Fig. 5B).
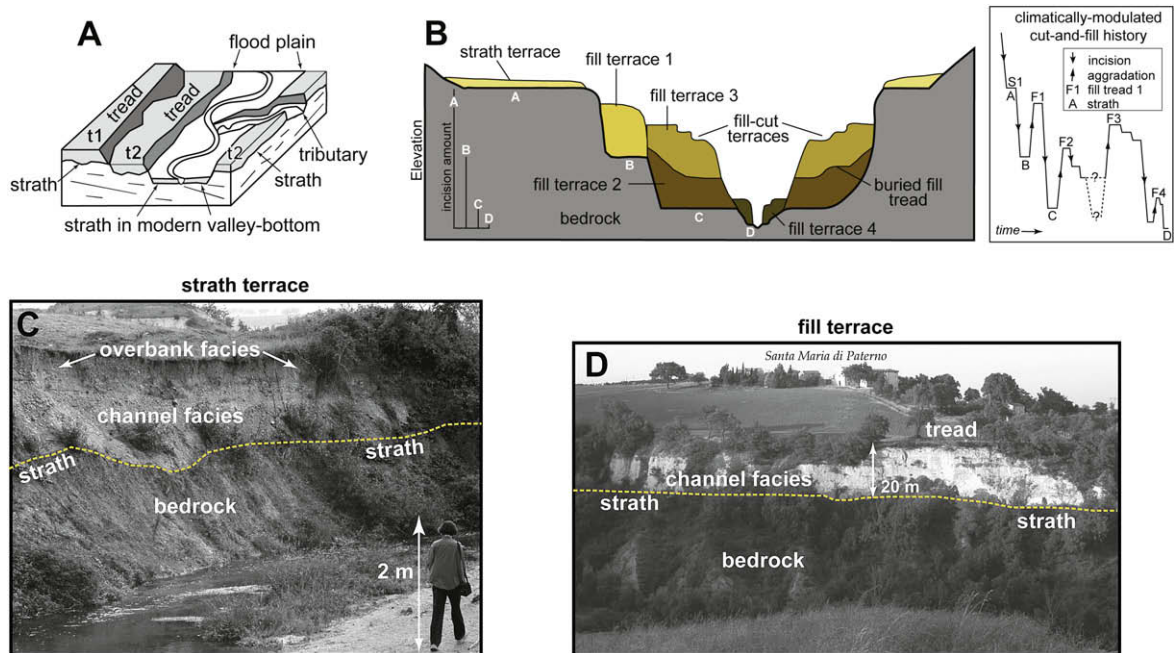
Fig. 5. Cartoon and photographic relationships between terraces, terrace deposits and incision–aggradation history as used in this study. A. Schematic diagram illustrating the relationships between terraces (t1, t2), straths, floodplain, and valley bottom. The correspondence between the width of the floodplain and the width of the valley bottom strath is often corroborated by exposure of the valley bottom strath in tributary channels, shown entering from the right part of the diagram (Wegmann and Pazzaglia, 2002). B. Hypothetical cross-section showing geometric differences between strath and fill terraces and an idealized complex sequences of fill (aggradational) and fill-cut (degradational) terraces. Strath surfaces labeled A–D are appropriate datums from which to measure the amount and rate of fluvial incision. With strath terraces it is generally assumed that the overlying sediment is intimately associated with the beveling of the strath surface and that the age of the overlying sediments can be used as a proxy for the age of the strath surface itself. For thick fill terraces, the age of the burying sediments may be thousands of years younger than the underlying strath. For proper determination of bedrock incision rates, the timing of strath beveling must be known or approximated. For fill terraces, a minimum strath age can be determined from the oldest radiometric age obtained from basal fill deposits. Multiple cut-and-fill events are outlined in the right-hand box corresponding to the amount of river incision into bedrock that can be determined from each terrace on the left-hand side of the cross-section (modified from Burbank and Anderson, 2001). C. Photograph of an exposure of Late Holocene strath terrace (Qt9) in the Musone River basin near San Vittore. The strath is beveled on Middle Pliocene marine clays and marls. D. Photograph across the valley of the Torbido River near Santa Maria di Paterno in the Potenza River basin of a 20–25 m thick fill terrace (Qt3) exposure. The strath is beveled on clays of the upper Miocene Colombacci Fm.

4.2. Strath genesis and application

The formation of straths appears to require a combination of complimentary factors including a relatively non-resistant bed (Wegmann, 1999; García, 2006), oscillatory fluxes of sediment and water (Meyer et al., 1995; Tucker and Slingerland, 1997; Hancock and Anderson, 2002; Hartshorn et al., 2002; Bogaart et al., 2003a,b), moderate-to-low rates of rock uplift (Finnegan et al., 2005), and a threshold drainage basin size (García, 2006). The conditions necessary to form wide preservable straths reduce to the ratio of lateral to vertical bedrock incision rate. This requires a period of relative vertical thalweg stability paired with horizontal thalweg mobility (e.g. sweeping meander loops), irrespective of the particular mechanism responsible for lateral bedrock planation (Gilbert, 1877; Hancock and Anderson, 2002; Wegmann and Pazzaglia, 2002; Montgomery, 2004). Montgomery (2004) and García (2006) showed that valleys can widen much faster than long-term vertical incision rates where bedrock at the water–air interface is susceptible to physical weathering by repeated wetting and drying.

Bedload plays a central role in carving straths, as it can act as both an abrasive and an insulator (Sklar and Dietrich, 1998; Hancock and Anderson, 2002). Relatively high sediment supply promotes wide valley floors and low effective water discharge maintains them. An over-supply of sediment results in aggradation and valley bottom burial. The transition from valley widening or aggradation to downcutting and terrace creation occurs in response to a decrease in sediment supply and/or greater effective discharge (Schumm, 1969; Hancock and Anderson, 2002), which on the timescale of an individual terrace are likely to be climatically driven (e.g. Bull, 1991; Meyer et al., 1995).

Observations from tectonically active settings demonstrate that straths lie at variable distances above the modern valley bottom, but their ages tend to cluster around periods coincident with known climatic change (Fig. 5B), prompting geomorphologists to appeal to the impacts of climate change as the main driver of the periodic incision necessary for terrace genesis (Bull and Knuepfer, 1987; Bull, 1991; Pazzaglia and Gardner, 1993; Merritts et al., 1994; Meyer et al., 1995; Burbank et al., 1996; Fuller et al., 1998; Pazzaglia et al., 1998; Hancock et al., 1999; Lavé and Avouac, 2001; Pazzaglia and Brandon, 2001; Pan et al., 2003).

The rate of fluvial incision into bedrock is commonly interpreted as the rate of rock uplift with the built-in assumption that strath formation is a shorter-term transient phenomenon embedded in a long-term quasi-equilibrium channel profile (Mackin, 1948) more or less represented by the gradient of the modern river profile (Knox, 1975; Bull and Knuepfer, 1987; Merritts et al., 1994; Personius, 1995; Burbank et al., 1996; Lavé and Avouac, 2000; Pazzaglia and Brandon, 2001; Wegmann and Pazzaglia, 2002). Straths occur in mountainous regions across a wide range of channel incision rates from ≤1 mm/yr where they are commonly paired and extensive (e.g. Japan, Sugai, 1993; Oregon Coast Range, Personius, 1995; California Coast Range, Merritts and Vincent, 1989; Olympic Mountains, Pazzaglia and Brandon, 2001; Nepalese Himalaya, Lavé and Avouac, 2001; New Zealand, Bull and Knuepfer, 1987; and the Apennines, Picotti and Pazzaglia, 2008) to as high as ∼10 mm/yr for rivers in rapidly uplifting regions (Burbank et al., 1996; Hartshorn et al., 2002), where they tend to be unpaired and have limited down-valley extent (<1 km).

The age of the axial channel gravel directly above the strath approximates the timing of strath carving and places constraints on the timing of strath terrace genesis (Wegmann and Pazzaglia, 2002) (Fig. 5C). Typically, the age of alluvium above a strath surface cluster around the time of strath abandonment, with a smattering of older ages representing the duration of the wide strath carving process (Wegmann and Pazzaglia, 2002). Although sediment wave propagation (Weldon, 1986) and/or knickpoint retreat (Seidl and Dietrich,

1992; Zaprowski et al., 2001) result in diachronous incision and strath abandonment, the duration of these processes in tectonically active settings is shorter than the variations in Quaternary climate driving the carving of major strath surfaces (Bull, 1991; Merritts et al., 1994; Pazzaglia and Brandon, 2001). Similarly, for fill terraces (Fig. 5D) a minimum strath age can be determined by the age of the stratigraphically lowest (oldest) alluvium directly atop the strath, assuming no reoccupation of the strath by a younger channel. Subsequent incision of the terrace fill deposit and underlying strath surface is approximated by the age of the youngest conformable terrace alluvium in the fill sequence.

Following Lambeck et al. (2004), determination of the fluvial incision rate (I) for a specific locality along the channel, which we utilize as a proxy for base level fall (rock uplift), is given by:

$$I = H_S/T_S, \tag{1}$$

where H_s is the height (m) of the bedrock strath above the modern channel, and T_s is the timing (ka) of strath preservation in the landscape. The uncertainty in incision rate (σ_I) is:

$$\sigma_I = \sigma_{H_s}/T_s^2 + (H_s/T_s)^2 \sigma_{T_s}, \tag{2}$$

where σ_{H_s} is the uncertainty in measured strath height (m) and σ_{T_s} is the uncertainty in the timing of strath preservation. Values of σ_{H_s} are generally ≤1 m for straths ≤10 m above the modern channel, 1–5 m for terraces ≤50 m above the channel, and 10 m for staths >50 m above the channel. Values of σ_{T_s} are based upon the numeric age uncertainty from radiocarbon dates or from correlation to the Marine Isotope Stage (described below).

4.3. Field and laboratory methods

Existing geologic maps, field exposures, air photos, topographic maps (1–5 m contour intervals), and 10-m digital elevation models (DEM) were used to identify fluvial terraces. The stratigraphy, sedimentology, petrology, and weathering characteristics, including soil profile development, are the primary lithostratigraphic criteria used to describe and correlate terraces. The height of bedrock strath surfaces above the modern channel was determined in the field from natural and man-made outcrops by means of a barometric altimeter accurate to ±1 m for straths >5 m above the channel (Data Repository DR-1 & DR-2). The heights of straths less than 5 m above the channel were measured with a stadia rod and level, accurate to ±0.1 m.

Bivalve and gastropod shell and detrital charcoal fragments were extracted from bulk sediment samples of interstitial sand collected between cobbles and from sandy lenses in otherwise coarse-grained axial channel facies terrace deposits. Where possible, samples were collected directly above a strath (e.g. Fig. 5C). AMS radiocarbon dating of these samples was completed at the University of Arizona and University of California Irvine labs. Uncalibrated ^{14}C ages are reported with one-sigma standard errors and converted to calendar years before present (ybp) with the Fairbanks0805 calibration program (Fairbanks et al., 2005).

Correlating terrestrial Quaternary sequences with the marine oxygen isotope record is now suitably well established (e.g. Bridgland and Westaway, 2008). We utilize the marine oxygen isotope record of Lisiecki and Raymo (2005) as a long-term framework for identifying likely times of strath cutting and channel aggradation or incision. In the absence of numeric ages, particularly from older terraces, we use the chronology of the marine isotope record as a best approximation for terrace strath age. In addition, we utilize terrace stratigraphies of nearby river valleys and their downdip-equivalent subsurface deposits beneath the southern Po Plain (Di Dio, 1998; Amorosi et al., 2004; Picotti and Pazzaglia, 2008) as further controls on strath age.

Channel longitudinal profiles extracted from the DEMs were projected to a common mid-valley reference profile and smoothed by applying a 1st-order polynomial LOESS tricube weighting routine with a kernel 0.1 times the river length in order to remove artificial steps. Terrace longitudinal profiles were generated by projecting the upstream distance from the river's mouth (0 km) to the same reference profile. Mapped faults and folds were digitized from existing sources (Pignone et al., 1994, 2001; Centamore et al., 1991; Bigi et al., 1992; Bonini, 2007) into a GIS database for comparison to terrace profiles. Rates of fluvial incision were determined at 10-km intervals along each river profile using equations (1) and (2).

Strath deformation, particularly where that deformation straddles the transition from the Apennines into the Po foreland, is constrained by well-known depths of subsurface marine, littoral and fluvial deposits correlative to the terrace deposits. Three identifiable littoral marker units, the Tyrrhenian beach (MIS 5e), pre-Tyrrhenian beach (MIS 11), and Imola sands (Sabbie di Imola – MIS 17–21), provide key temporal and vertical control for the subsurface data (Di Dio, 1998; Amorosi et al., 1998b, 2004). Deformation can be described as the vertical uplift or subsidence with respect to a regional datum that is defined by sea level and the local channel or depositional system gradients across a 40 km-long baseline, assumed to have been more or less constant over the stratigraphic age of the deformed horizons. If all of the observed deformation was accommodated by a single emergent fault, the slip rate (ds/dt) in mm/yr can be described by:

$$\frac{ds}{dt} = \frac{H}{(\sin \alpha)t} 1000, \qquad (3)$$

where H is the height (m) above stratigraphic regional, α is the dip of the fault, and t is the age of the deposits in years (Hardy and Poblet, 2005). Equation (3) does not account for horizontal partioning of strain, sediment compaction, isostatically driven subsidence in the Po Plain, or long-wavelength flexural loading of the crust and can only be used to measure maximum values of fault slip, as some of the observed deformation might be distributed among these or related causes.

5. Results

5.1. Bidente basin

5.1.1. Terrace stratigraphy and chronology

Our terrace numbering scheme, from Qt0 to Qt9, represents a unified inter-basin chronostratigraphy that results from climate modulation of hillslope and fluvial geomorphic processes through variable sediment discharge (Fig. 7). The functional benefit of cross-basinal correlation available with this scheme outweighs the disadvantage imposed by different numbers of terraces in the basins studied (see Section 5.2.1 below).

We map nine strath terraces in the Bidente basin that share similar sedimentologic and geomorphic characteristics to those described for the Reno and adjacent basins near Bologna (Amorosi et al., 1996; Picotti and Pazzaglia, 2008) (Figs. 1, 6 and 7). At the outcrop scale each terrace consists of a planar bedrock strath surface with ~1 m of local relief, above which are 3–5 m of upwards fining alluvial gravel and sand. The alluvium consists of 1–3 m of well-bedded and imbricated axial channel gravels overlain by 1–3 m of horizontally bedded-to-trough cross-stratified pebbly sand-to-silt that becomes massive and bioturbated towards the top with an increasing degree of pedogenesis concomitant with terrace age (e.g. Eppes et al., 2008) (Fig. 6). Terrace alluvia are overlain by post-terrace colluvial and alluvial fan deposits that tend to increase in thickness with terrace age and proximity to tributary mouths and valley margins.

The topographically highest and oldest river deposits, named Qt0, are limited to scatted outcrops of weathered, rounded and matrix-supported alluvial gravels atop low-relief isolated drainage divides, out of the context of the modern Bidente valley (Fig. 6). These high old terrace remnants are likely fluvial equivalents to the Imola Sand (IMO) deposits of the Po foreland. The Imola Sands constitute at least three conformable progradational, coarsening-up allostratigraphic packages (IMO 1–3) that record marine-littoral followed by fan-delta deposition during interglacial to glacial climate cycles in the Late Early and Middle Pleistocene (Amorosi et al., 1998b; Di Dio, 1998). Martelli et al. (2008) and Picotti and Pazzaglia (2008) document excellent along-strike mountain front exposures near Bologna that clearly show a marker horizon such as IMO 1 rising out of the Po Plain, coarsening-up dip, and becoming a mapped terrace (Qt0) at the apex of a mountain front flatiron. The main body of the Imola Sands, IMO 1, is numerically constrained to 780–990 ka by paleomagnetic and 800 ± 10 ka by electron spin resonance analyses from an archeological site at Monte Poggiolo, 5 km southwest of Forli (Antoniazzi et al., 1993; Fig. 3). Four additional ^{10}Be cosmogenic burial dates of 900 ± 100 were recently obtained from quarry exposures of IMO 1 at Castel San Pietro (Fig. 1) (Cyr and Granger, 2008). Available age constraints on IMO 1 help to confine the interval of Qt0 deposition to MIS 22–18, the glacial periods between the three intervening interglacials of MIS 21, 19, and 17 (Fig. 7); a time during which the mountain front first emerged as a topographic feature. In the Bidente basin, IMO units do not crop out; however, they are identified in three wells between the mountain front and the Adriatic coast (Di Dio, 1998) (Fig. 8). The Qt0 strath increases in height above the river from 89 m at the mountain front to a maximum of 428 m at valley km 28 (Data Repository DR-1).

Paired strath terraces Qt1 and Qt2, located along the outer valley margins, help to define an Early Middle Pleistocene Bidente valley. Outcrops of these terraces, isolated to the tops of hills and low-relief surfaces (Fig. 6), are evidence for ongoing incision and localized topographic inversion since their deposition in the valley bottom. Qt1 and Qt2 alluvium is poorly exposed, often consisting of weathered and rounded sandstone clasts in a clay-rich matrix on low-relief benches. An exception to this observation is the outstanding exposure of a Qt2 deposit preserved in a 185 m high cliff face along the Bidente River opposite the town of Galeata (Figs. 3 and 6). Here, the 175-m high Qt2 strath cuts across Miocene turbidities of the Marnoso Arenacea Fm and is overlain by 3–5 m of axial channel deposits, which in turn are overlain by a ≥10 m thick polygenetic colluvial wedge with paleosols and a deep weathering profile with the reddest (5YR) pedogenic colors observed in the basin (Fig. 6). Qt1 straths increase in height above the modern Bidente channel from a low of 86 m at 3.5 km from the mountain front to a high of 315 m at valley km 30.5. Similarly, Qt2 straths increase from a height of 41 m at the mountain front to 190 m at valley km 30.

Numeric ages do not exist for Qt1 or Qt2 deposits; however, downdip progradational alluvial fans beneath the Po Plain indicate that the Qt1 and Qt2 straths were beveled between the eustatic highstands responsible for deposition of IMO 1–3 units (MIS 21–17) and a pre-Tyrrhenian highstand beach (MIS 11) preserved in the Po subsurface in front of the Bidente valley mouth (Fig. 8) (Di Dio, 1998; Picotti and Pazzaglia, 2008). Based upon these stratigraphic relationships, Qt1 is assigned to a strath formation age of 620 ± 30 ka consistent with cutting during MIS 16, a significant glacial period based upon the MIS proxy record (Lisiecki and Raymo, 2005). Similarly, Qt2 is assigned to the next significant glacial stage, MIS 12 at 440 ± 50 ka. The rather large uncertainty associated with the Qt2 age indicates that it or part of it may also represent strath cutting during MIS 11–10 instead (Fig. 7).

Qt3 represents one or more straths underlying a prominent valley bench that separates scattered and poorly exposed older terraces from nearly contiguous exposure of the inset Late
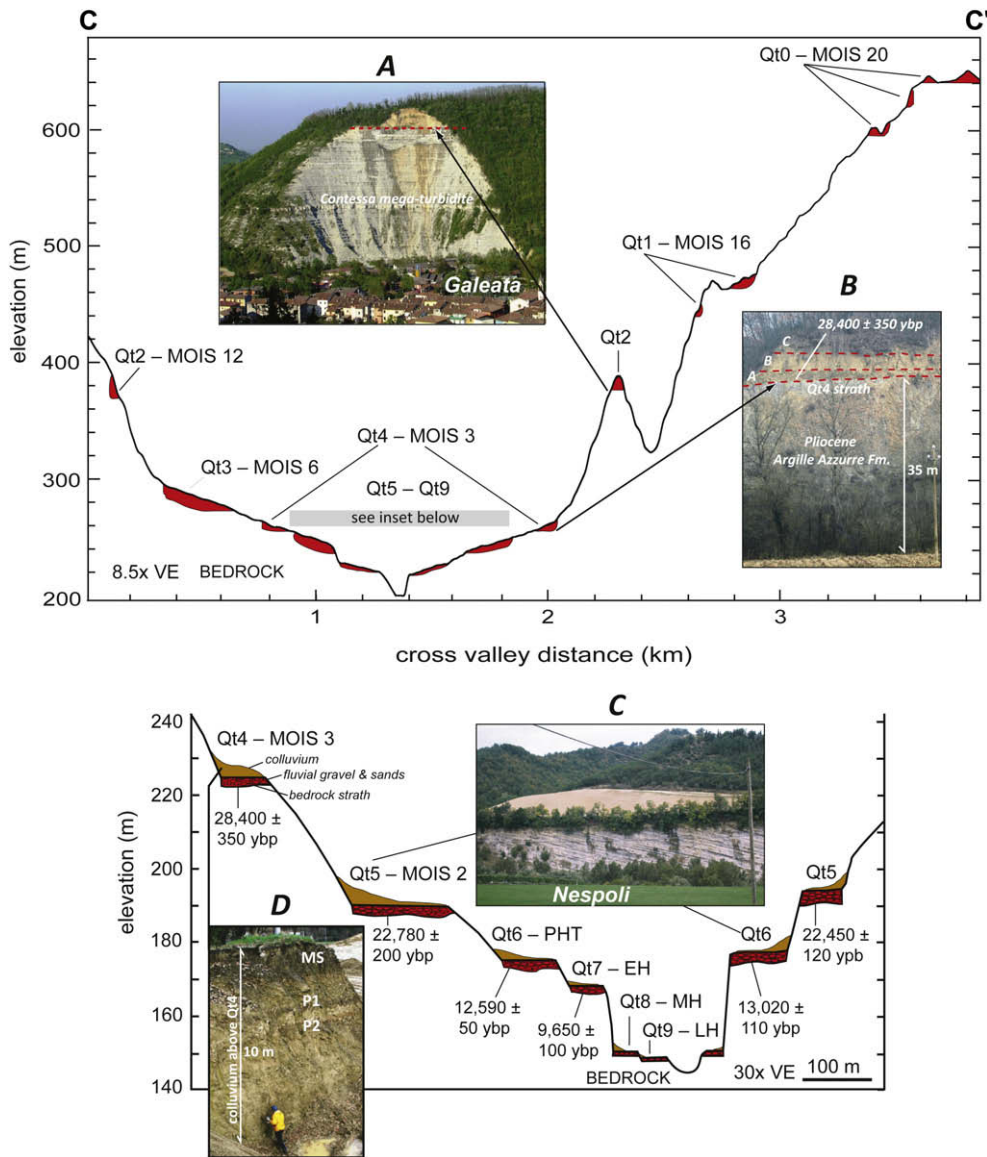
Fig. 6. Composite topographic profile (C–C′, Fig. 3) and cross-section at Bidente valley km 27 showing the spatial distribution of fluvial terraces and the inferred marine Oxygen Isotope Stage (MIS) during which the strath surfaces were carved. Top: overall distribution and nomenclature for the Bidente basin strath terraces; vertical exaggeration = 8.5. Inset photo A: Qt2 deposit above the town of Galeata at valley km 25, the strath of which is ~175 m above the modern channel. In this exposure, 3–5 m of axial channel gravels are overlain by 10–15 m of finer-grained younger colluvial deposits. The Middle Miocene Galeata member of the Marnoso Arenacea Fm (Pignone et al., 1994) is exposed in the cliff face and the single, thick sandstone layer visible one-third of the distance from the base of the cliff is the 7–8 m thick "Contessa" mega-turbidite. The Bidente River, located at the base of the rock slope, is not visible. Inset photo B: Typical exposure of a 35 m high Qt4 strath terrace deposited on top of Pliocene marine Argille Azzurre Fm mudstones. Unit A is a 1–1.5 m thick axial channel gravel with a calibrated ^{14}C age of 28,400 ± 350 ybp, unit B is 3 m of fluvial sands fining upwards to silty overbank deposits, and unit C consists of younger colluvial deposits burying the original terrace tread. Bottom: Inset of Late Pleistocene-to-Holocene terrace relationships, the stratigraphic position of radiocarbon ages form this study, and interpreted climatic intervals during which straths were carved; PHT = Pleistocene-to-Holocene transition, EH = Early Holocene, MH = Middle Holocene, LH = Late Holocene; vertical exaggeration = 30×. Inset photo C: view to the west from the tread of Qt6 across the incised Holocene valley of the Bidente River to an exposure of the Qt5 terrace at valley km 19, near Nespoli. The Qt5 terrace is cut across north-dipping Miocene turbidites of the Nespoli member of the Marnoso Arenacea Fm (Pignone et al., 2001). The terrace deposit consists of 2–3 m of axial channel sands and gravels that have a calibrated ^{14}C age of 22,780 ± 200 ybp overlain by 4–5 m of colluvium. The Qt5 strath is 36 m above the modern channel (not visible). Inset photo D: exposure of colluvial wedge on top of Qt4 deposits at valley km 29. Over 10 m of clay-rich gravelly colluvium buries Qt4 deposits. Two distinct buried paleosols (P1, P2), each ~1 m thick, are exposed beneath the modern soil (MS), and may correlate to the Qt5 and Qt6 terrace forming intervals, respectively.

Pleistocene and Holocene terraces (Figs. 6 and 8). Exposures of Qt3 alluvium are rare with road cuts commonly showing only the thick accumulation of colluvial and alluvial fan deposits that bury the terrace inner angle tread. At the mountain front, the Qt3 strath is 30 m above the modern channel, increasing in height to 123 m at 31.5 km upvalley. Terraces from Qt0 to Qt3 are not preserved in the landscape upstream of valley km 32 (Fig. 8). The Qt3 strath is assigned to an age of 140 ± 10 ka (MIS 6) based upon downdip correlation to alluvial fan deposits beneath the Po Plain that lie between the MIS 11 and MIS 5e (Tyrrhenian) eustatic highstands (Fig. 8; e.g. Di Dio, 1998; Amorosi et al., 2004; Picotti and Pazzaglia,

2008). An angular unconformity separates the Qt3-equivalent deposits beneath the Po Plain from the transgressive marine and beach sediments associated with the Tyrrhenian eustatic highstand at ~123 ka (Amorosi et al., 2004).

Terraces Qt4–Qt9 represent a greater fidelity in the genesis and preservation of straths during the Late Pleistocene than the ~100 ka periods represented by Qt0–Qt3. Straths and deposits of these younger terraces are well exposed along the river's cut banks and lower reaches of tributary streams.

Soils developed within Qt7–Qt5 terrace deposits show a progressive increase in the amount of pedogenic carbonate with
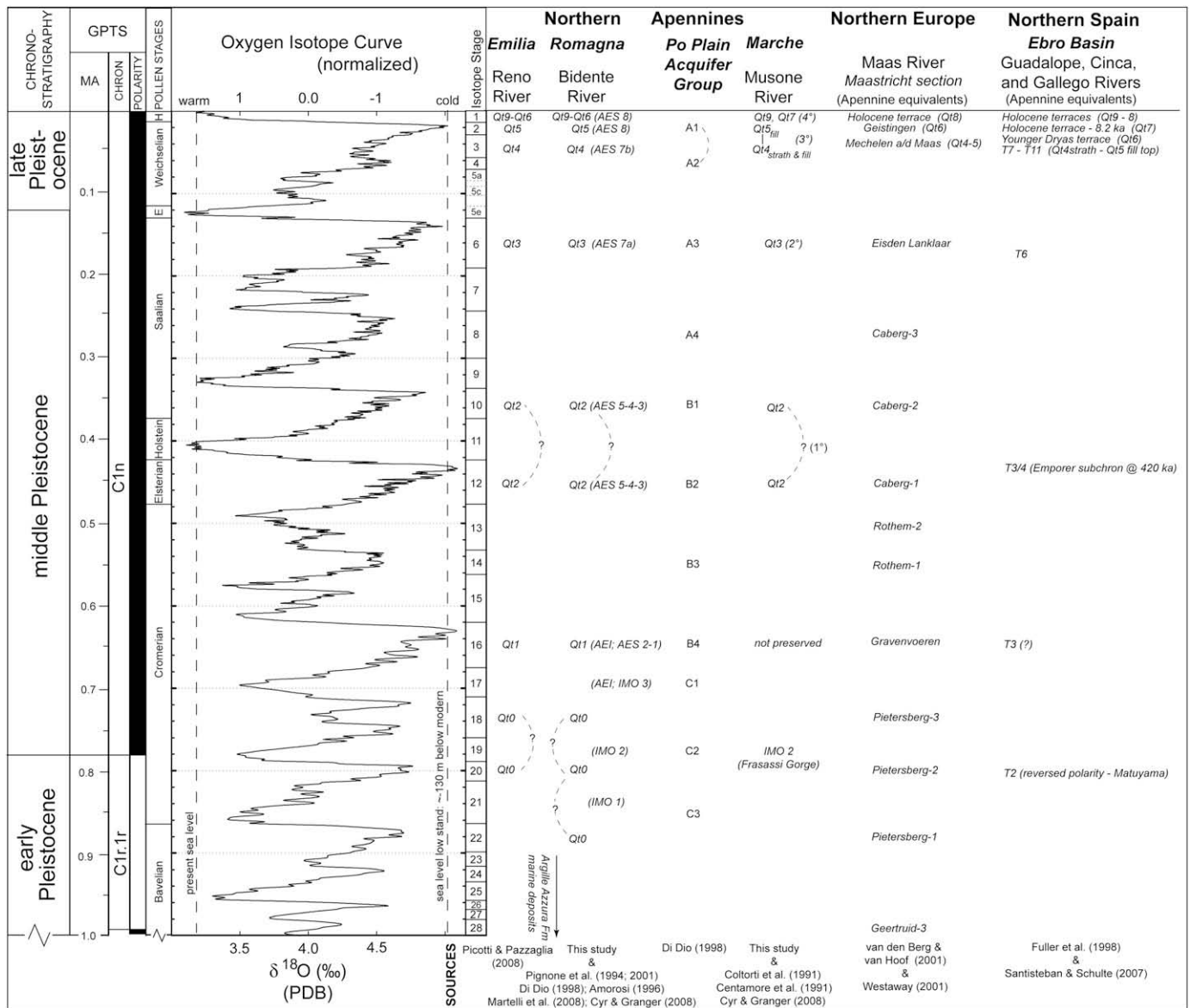
Fig. 7. Chronostratigraphic correlation diagram for fluvial and near-shore marine deposits of the Romagna and Marche Apennines mapped onto the oxygen isotope curve of Lisiecki and Raymo (2005) and placed into a common nomenclature for the Bidente and Musone basins. The extensive terrace stratigraphy for both the Maastricht section of the Mass River in SE Netherlands (van den Berg and van Hoof, 2001) and the Ebro basin in Spain (Fuller et al., 1998; Santisteban and Schulte, 2007) are provided for comparison. Parenthetical designations for the Bidente River column are for terrace-equivalent alluvial deposits beneath the Po Plain; AEI = Emiliano-Romagnolo Inferiore Synthem; AES = Emiliano-Romagnolo Superiore Synthem (Di Dio, 1998); IMO = Imola Sand Fm (Sabbie Gialle) (Martelli et al., 2008). Parenthetical designations for the Musone River column indicate previously utilized terrace nomenclature (e.g. Coltorti et al., 1991 and Centamore et al., 1991). For the Ebro basin record, the Holocene – T6 terraces are from the Guadalope basin (Fuller et al., 1998); T3/4 and T2 are from the Gállego and Cinca basins, respectively (Santisteban and Schulte, 2007). GPTS = geomagnetic polarity timescale and ACN = Aquifer Complex Number (Complesso Acquifero) corresponding to Po subsurface deposits of the Emilia–Romagna Region (Di Dio, 1998). The age of Imola sands (IMO 2), MIS 19, ("Sabbie Gialle") in the Romagna area is provided by electron spin resonance and paleomagnetic measurements to 0.80 ± 0.1 and 0.780–0.990 Ma, respectively (Antoniazzi et al., 1993). Fluvial deposits preserved in caves from the Frasassi Gorge (Gola di Frasassi), interpreted as being continental equivalents to the Imola sands (IMO 2), yielded a cosmogenic burial age of 0.75 ± 0.026 Ma (Cyr and Granger, 2008).

terrace age. The Qt7 terrace exhibits a stage I carbonate morphology (Birkeland, 1999), with coatings of roots and ped faces in fine-grained soils, and as minor coatings on the underside of gravels. Qt6 soils exhibit stage II carbonate morphology with carbonate pendants on the bottoms of gravels and disseminated carbonate throughout the Btk horizon. Qt5 deposits display stage II+ to III morphology with thick accumulations of carbonate on the bottoms of all clasts, a distinct Bk horizon, and 2–3 mm nodules of carbonate throughout the lower half of the soil profile. Soils developed on terraces older than Qt5 lack significant accumulations of carbonate, similar to trends documented for the terrace sequence of the Reno River (Eppes et al., 2008). Two buried

paleosols were observed within a 10 m deep construction-site exposure in colluvium on top of a Qt4 terrace 2.25 km north of Santa Sofia (Figs. 3 and 6). The 2-m thick paleosols may represent Qt5 and Qt6 equivalent soils buried by pulses of colluvial deposition onto the Qt4 tread.

As with the older terraces, Qt4 though Qt7 show a progressive increase in strath height above the modern channel away from the mountain front. Qt4 increases from 30 m at 3.4 km to a maximum of 67 m at 38 km upvalley. Qt5 increases from 15 m at 5 km from the mountain front to 43 m at 25 km upvalley. Qt6–Qt7 are at 14 and 11 m respectively at 8.9 km from the mountain front and 28 m and 21 m at 29 and 22 km up valley.
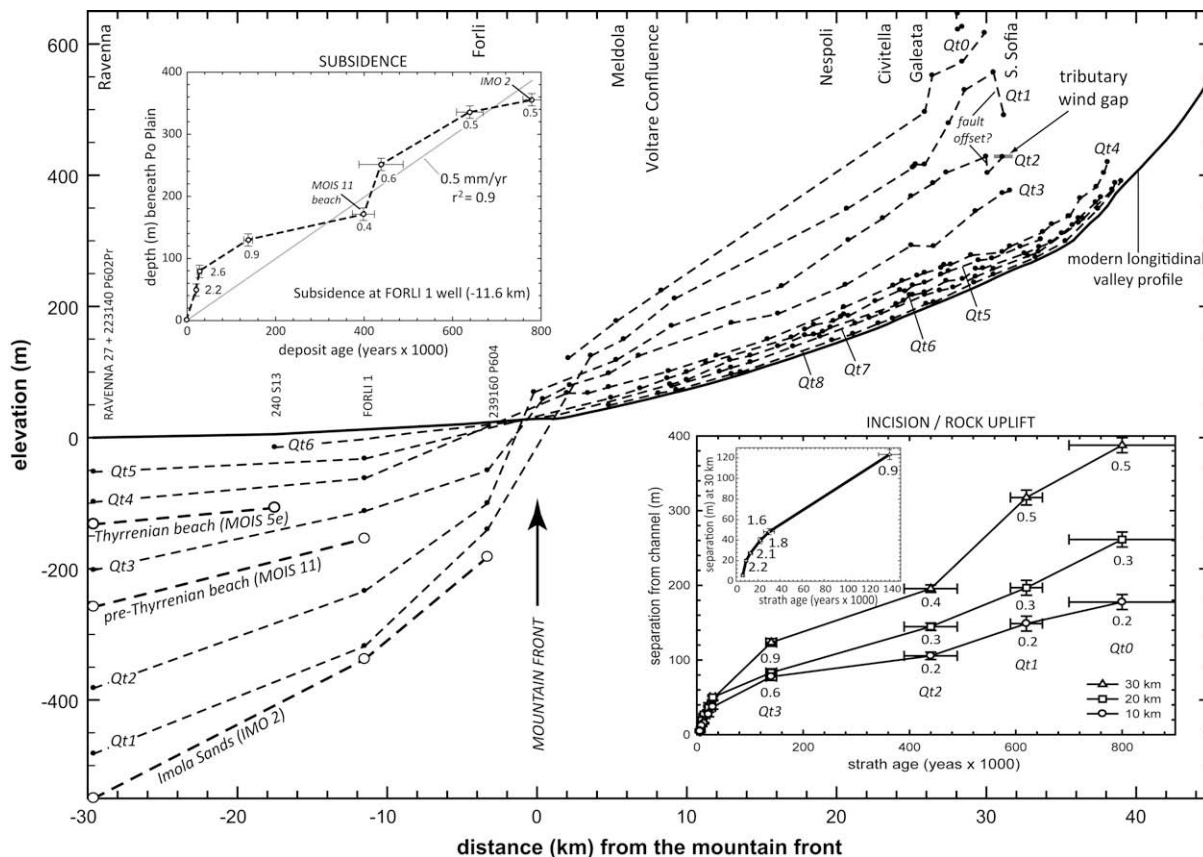
Fig. 8. Projection and correlation of reconstructed Bidente River terrace strath surfaces across the mountain front and into the Po subsurface. The solid black line is the modern Bidente longitudinal profile. Solid circles along the profiles indicate locations of measured bedrock strath elevations projected to the modern longitudinal profile. Numbers on inset graphs are fluvial incision or basin subsidence rates in mm/yr. Subsurface data are from oil and water well logs (labeled) compiled by Di Dio (1998) and Amorosi et al. (2004). MIS = Marine Oxygen Isotope Stage, used for climatic tuning of subsurface deposits to the Tyrrhenian and pre-Tyrrhenian sea level highstands. The age of the Imola sands (IMO 2), encountered in subsurface wells beneath the Po Plain, exposed along the mountain front 5 km to the west–southwest of Forli, and correlated to the Qt0 terrace surface in the Bidente basin, is constrained by electron spin resonance and paleomagnetic measurements to 0.80 ± 0.1 and 0.780–0.990 Ma, respectively (Antoniazzi et al., 1993), likely correlating to Oxygen Isotope Stage 19. Evidence of fault offset of Qt1 and a tributary wind gap graded to the Bidente River during Qt2 time is coincident with a ~10 km-long upstream convergence of the Qt4–Qt8 longitudinal profiles near Santa Sofia (Fig. 9).

Dating material collected from the Late Pleistocene terraces provides the first calibrated ^{14}C ages reported for the Bidente basin (Fig. 3; Table 1). Qt4 yielded a single age of 28,400 ± 350 ybp and the strath is assigned to an age of 30 ± 5 ka, or latest MIS 3. Two dates from a single outcrop of Qt5 yielded deposit ages of 22,780 ± 200 and 22,450 ± 120 ybp, correlating to a minimum Lateglacial Maximum (MIS 2) age of strath formation at 22 ± 2 ka (Fig. 7). Three dates from Qt6, two from the Bidente basin and one from the adjacent Savio River basin (Fig. 4) constrain a narrow interval of strath beveling and deposit emplacement between 13,030 ± 100 and 12,590 ± 50 ybp. A single age from Qt7 yielded an Early Holocene age of 9650 ± 110 ybp (Fig. 7; Tables 2 and 3).

A 100-to-200-m wide Holocene valley, containing two mappable strath terraces (Qt8–Qt9), is inset into the latest Pleistocene valley (Fig. 6). Qt8 increases in height above the river from 4 m at 4.8 km from the mountain front to a maximum of 11 m above the channel at 37.5 km upstream. The height of Qt9 is everywhere ≤5 m above the channel. These two terraces were not dated in the Bidente basin; however, similar terraces in the Reno valley yield calibrated ^{14}C ages between 6410 ± 50 to 6120 ± 80 and 1930 ± 70 to 1050 ± 50 for the Qt8 and Qt9 deposits (Eppes et al., 2008), which are assigned to Middle and Late Holocene ages for strath beveling, respectively (Table 2). Separation of Qt9 from the channel may be a response to anthropogenic impacts in the Bidente basin, including gravel bed mining, an activity documented for many other northern Apennine rivers (Brugnara and Zannoner, 1997).

5.1.2. Terrace longitudinal profiles and incision rates

Reconstructed terrace longitudinal profiles diverge upstream from the modern valley profile (Fig. 8). Near the mountain front, all terraces project downdip into equivalent subsurface alluvial fan deposits (Di Dio, 1998; Picotti and Pazzaglia, 2008) across a short distance of not more than several kilometers (Figs. 7 and 8). The longitudinal profiles of Qt4–Qt8 converge towards the modern channel beginning at valley km 28 and extending upvalley to km 40, above which terrace preservation is too sparse to allow for robust profile reconstructions. This example of upstream convergence is coincident with offset Qt1 and Qt2 straths adjacent to down-to-the south faults at about valley km 30 (Fig. 8).

Rates of fluvial incision determined at 10-km increments, using equations (1) and (2), increase upstream from the mountain front (Fig. 8). The rates for Qt0 through Qt2 vary little from 0.2 mm/yr at 10 km to 0.5 mm/yr at 30 km. The incision rates calculated from Qt3 approximately double over the previous ~650 ka to 0.6–0.9 mm/yr (Fig. 8; Table 2). Incision rates continue to accelerate to 1.6–2.2 mm/yr for Qt4 through Qt7 (Fig. 8). A similar twofold increase is observed between Reno valley Qt2 and Qt3 straths (Picotti and Pazzaglia, 2008). In comparison, Po Plain subsidence rates calculated from the elevation of deposits in the FORLI 1 well located 11.6 km north of the mountain front vary between 0.4 and 0.6 mm/yr between ~780 ka (IMO 2) and 400 ka (MIS 11 beach). Subsidence increases from 0.9 mm/yr at 140 ka (Qt3) to 2.6 mm/yr at 30 ka (Qt4) (Figs. 7 and 8; Table 2).

Table 1
New ^{14}C ages for fluvial deposits of the Bidente River valley.

Fig. 3A ID #	Lab ID[a]	Lat (°N)	Long (°E)	Material	δ^{13}C (‰)	[14]C age (years)	Calibrated[b] 1σ min (yr BP)	Calibrated[b] (yr BP)	Deposit
1	AA64959	43.976	11.908	shells	−6.9	8700 ± 70	9760	9550	Qt7
2	AA65341	44.030	11.983	shells	−6.5	10,600 ± 60	12,650	12,540	Qt6
3	AA64966	44.001	11.935	shells	−6.9	11,090 ± 70	13,130	12,900	Qt6
4	AA65342[c]	43.910	12.124	shells	−6.7	11,100 ± 60	13,130	12,920	Qt6
5	AA65340	44.131	12.074	shells	−5.8	18,870 ± 140	22,560	22,330	Qt5
6	AA65340r[d]	44.131	12.074	shells	−5.8	19,180 ± 130	23,000	22,570	Qt5
7	AA65339	44.091	12.087	shells	−4.7	23,840 ± 320	28,750	28,050	Qt4

[a] All samples analyzed at the University of Arizona Accelerator Mass Spectrometry Laboratory.
[b] All ^{14}C ages were calibrated using the Fairbanks0805 radiocarbon calibration curve (Fairbanks et al., 2005).
[c] Sample from Qt6 deposit in Savio River basin (Fig. 3).
[d] Replicate of sample AA65340.

5.1.3. Evidence for active faulting from the terrace record

Evidence for fault offset of terraces in the Bidente basin is present near valley km 30 (Figs. 8 and 9) where the Qt2 strath is offset ∼25 m and the Qt1 strath is offset ∼65 m. If accommodated by a single dip-slip fault (Bonini, 2007), the slip rate would vary from 0.05 to 0.1 mm/yr for the past 440–620 ka, respectively. A wind gap at the height of the Qt2 terrace (185 m) separates the Torto and Bidente Rivers along the inferred trace of the fault (Figs. 8 and 9). Similarly, obvious knickpoints in the Torto profile correlate with Qt2–Qt5 terrace elevations. The longitudinal profile of the Torto River is concave above the wind gap and slightly convex below. The steepness and concavity of the upper portion of the Torto profile is more similar to adjacent streams draining to the Bidente than to its own profile below the elevation of Qt2 and the wind gap (Fig. 9).

5.2. Musone basin

5.2.1. Terrace stratigraphy and chronology

The Musone basin contains a suite of paired Middle Pleistocene-to-Holocene fill terraces depicted on Italian maps as 1st (Middle Pleistocene) through 4th (Holocene) order. Most of the rivers in the Marche region draining the calcareous Apennines have this characteristic suite of four paired fill terraces (e.g. Lipparini, 1939; Villa, 1942; Nesci and Savelli, 1990; Coltorti et al., 1991), attesting to at least four protracted periods of basin-wide aggradation during glacial intervals followed by valley incision and floodplain narrowing during ensuing periods of climatic transition into interglacial intervals (Alessio et al., 1979; Nesci and Savelli, 1990; Coltorti et al., 1991). These observations contrast sharply with the distinct lack of fill terraces for the Bidente and other Romagna Apennine streams (Picotti and Pazzaglia, 2008).

Musone fill terraces consist of thick (∼15 m) deposits of limestone-dominated clast-supported pebble-to-cobble gravels with occasional lenses of sand and silt, and common shells of freshwater gastropods. Extensive stratified colluvial and alluvial fan deposits interfinger with the terrace alluvium (Coltorti and Dramis, 1995; Savelli et al., 1996). Straths buried by the fill are locally exposed, especially along the San Vittore reach (valley km 27–35) and within Cingoli Gorge (Fig. 4). Tread soils display a progressive thickening of pedogenic clay in the B-horizon and increasing reddening with terrace age.

Table 2
Bidente Terrace and Po Plain stratigraphy, ages, and rates of river incision and basin subsidence.

Terrace	Regione Map[a]	Po Plain Aquifer Group[b]	MIS[c]	Strath Height[d] Above Channel (m)	Depth[e] of Po Plain deposits (m)	Age (ka)	Incision Rate (mm/yr)	Subsidence Rate (mm/yr)	Source[f]
Qt9	AES 8a	A1	1	2.5 ± 0.5	n/a	1.5 ± 0.5[f]	1.7 ± 0.4	n/a	[14]C
Qt8	AES 8a	A1	1	6 ± 1	n/a	6 ± 1[f]	1.0 ± 0.1	n/a	[14]C
Qt7	AES 8	A1	1	20 ± 2	n/a	9 ± 1[f]	2.2 ± 0.1	n/a	[14]C
Qt6	AES 8	A2	2	27 ± 3	n/a	13 ± 2[f]	2.1 ± 0.2	n/a	[14]C
Qt5	AES 8	A2	2	40 ± 5	−48 ± 5	22 ± 2[f]	1.8 ± 0.1	2.2 ± 0.1	[14]C
Qt4	AES 7b	A2	3 (4?)	48 ± 5	−78 ± 5	30 ± 5[f]	1.6 ± 0.1	2.6 ± 0.2	[14]C
Qt3	AES 7a	A3	6	123 ± 10	−128 ± 5	140 ± 10	0.9 ± 0.01	0.9 ± 0.1	Amorosi et al. (1996), Di Dio (1998), Martelli et al. (2008)
MIS 11 beach	AES 6	B1	11	n/a	−170 ± 5	400 ± 10	n/a	0.4 ± 0.0003	Di Dio (1998)
Qt2	AEI; AES 5-4-3	B3-B2-B1	12-10	196 ± 10	−250 ± 5	440 ± 25	0.4 ± 0.003	0.6 ± 0.004	Di Dio (1998), Martelli et al. (2008)
Qt1	AEI; AES 2-1	B4	16	318 ± 10	−334 ± 5	620 ± 25	0.5 ± 0.001	0.5 ± 0.001	Di Dio (1998), Martelli et al. (2008)
Qt0/Qsi	IMO 3-1	C3-1	18-22	388 ± 10	−354 ± 5	700–900	0.5 ± 0.004	0.5 ± 0.0004	Antoniazzi et al. (1993), Amorosi et al. (1998b), Martelli et al. (2008), Cyr and Granger (2008)

[a] AEI = Emiliano-Romagnolo Inferiore Synthem; AES = Emiliano-Romagnolo Superiore Synthem; Qsi & IMO = Imola Sand Fm (Sabbie Gialle); Martelli et al. (2008).
[b] Di Dio (1998).
[c] MIS = Marine Isotope Stage.
[d] Strath elevations and rates of river incision are from terraces in the vicinity of Galeata, ∼30 km upvalley from the mountain front.
[e] The reported depth of deposits beneath the modern Po Plain surface are from the Forli 1 Well (Di Dio, 1998; Amorosi et al., 2004), 11.6 km north of the mountain front (Fig. 8).
[f] Average calibrated ^{14}C ages from multiple dates reported.

Table 3
New ^{14}C ages for fluvial deposits of the Musone River valley.

Fig. 4A ID #	Lab ID[a]	Lat (°N)	Long (°E)	Material	δ^{13}C (‰)	[14]C age (years)	Calibrated[b] 1σ max (yr BP)	Calibrated[b] 1σ min (yr BP)	Deposit
8	AA64963	43.439	13.248	Shells	−6.8	7970 ± 50	8980	8730	Qt7
9	AA64961	43.393	13.184	Shells	−4.7	16,730 ± 90	20,030	19,700	Qt5
10	AA64964	43.393	13.178	Shells	−7.1	23,020 ± 170	27,730	27,340	Qt5
11	AA64965	43.458	13.299	Shells	−9.3	>24,800	n/a	>28,570	Qt4–5
12	AA65338	43.429	13.234	Shells	−7.5	25,260 ± 210	30,780	30,160	Qt4–5
13	UCI21619	43.458	13.299	Shells	−2.9	26,540 ± 90	31,650	31,460	Qt4–5
14	AA646962	43.429	13.234	plant matter	−28.1	26,810 ± 290	32,020	31,530	Qt4–5
15	UCI21620	43.429	13.234	charcoal	−22.5	30,980 ± 240	36,240	35,580	Qt4–5

[a] Samples AA# were analyzed at the University of Arizona Accelerator Mass Spectrometry Laboratory. Samples UCI# were analyzed at the University of California Irvine W.M. Keck Carbon Cycle Accelerator Mass Spectrometry Laboratory.
[b] All ages were calibrated using the Fairbanks0805 radiocarbon calibration curve (Fairbanks et al., 2005).

The oldest and highest fill terrace preserved in the Musone basin is Qt2 (Figs. 7 and 10); terraces Qt0 and Qt1 are known for adjacent Marche rivers, but not in the Musone. Qt2 consists of about 15 m of poorly exposed gravels preserved in plowed fields on tributary ridges 50–75 m below the northern drainage divide from valley km 27.5–31. Along this reach, the height of the Qt2 strath, beveled on Upper Pliocene to Lower Pleistocene marine mudstones, increases from 60 to 90 m above the modern channel (Fig. 11) (Data Repository DR-2). There are no radiometric age determinations from Qt2 deposits; however, they are positioned stratigraphically lower than Qt0 and Qt1 equivalent deposits in adjacent basins and higher than the radiocarbon dead alluvium of Qt3 (see below). For example, in the adjacent Esino River, Qt0 equivalent cave deposits at Frasassi, ([10]Be burial age, 750 ± 260 ka; Cyr and Granger, 2008) and down-dip IMO-equivalent littoral deposits (Centamore et al., 1991) from near the mouth of the Musone River at Castelfidardo and Monte San Pellegrino ([10]Be burial age, 900 ± 100 ka; Cyr and Granger, 2008) are higher in elevation than Qt2 of the Musone basin. Following a glacio-climate origin and genetic symmetry with terraces elsewhere in Italy including the Bidente basin, we assign an MIS 12 or 10 age (440 ± 50 ka to 350 ± 50 ka) to the time of burial of the Qt2 strath (Fig. 7).

Inset below Qt2, Qt3 represents the remnants of the Late Middle Pleistocene Musone valley (Fig. 10). The terrace is best expressed as subtle topographic benches underlain by calcareous gravels in mid-slope positions downstream of the Marche and Cingoli ridges, and to tributary alluvial fan deposits that are now sub-basin topographic divides above Cingoli Gorge (e.g. Savelli et al., 1996) (Fig. 4). Typical Qt3 exposures consist of about 15 m of clast-supported alluvium overlain by several meters of colluvium. The Qt3 soil is 1.5–2 m thick with a well-developed Bt horizon and 10R 3/4 dusky red (Munsell) color. Where Qt3 grades into tributary alluvial fan facies, it locally thickens to 25 m. The Qt3 strath was identified in five localities along the Musone valley, the height of which increases in the San Vittore reach from 25 to 66 m. Within the Cingoli Gorge (valley km 42) the Qt3 strath is slightly lower at 60 m above the modern river, whereas at Chigiano (valley km 53.5) it has decreased in height to 40 m above the modern channel, which is on bedrock (Fig. 11) (Data Repository DR-2).

In situ chert artifacts interbedded with axial channel gravels were recovered from a 10-m high partial exposure of a Qt3 fill deposit near Chigiano (43.3031°N, 13.1446°E) (Fig. 10). The artifacts, tentatively identified as Middle Paleolithic-type products (possibly of an early facies of the Levallois Mousterian period C. Runnels, Boston University, pers. comm., 2008), share affinities with other hominin tools recovered from the Marche region assigned to an Early-to-Middle Paleolithic age (Paolo Appignensi, La Biblioteca Comunale di Cingoli, pers. comm., 2004; Peola, 1940; Cavelli, 1999). Collectively, the tentative correlation of these artifacts to the Middle Paleolithic, carbon materials beyond ^{14}C dating from Qt3 in

the Musone and adjacent basins (Calderoni et al., 1991; Nesci et al., 1995), and travertine uranium-series ages from Qt3-equivalent deposits in the nearby Frasassi Gorge (Taddeucci et al., 1992) support an age designation of >100 ka for the Qt3 deposits, consistent with a MIS 6 age of 140 ± 10 ka (Fig. 7).

Inset into Qt3 is Qt4–5, the most prominent and widespread fill terrace (3rd-order) in the Musone basin (Figs. 7 and 10). The calcareous gravels of Qt4–5 are 15–30 m thick, the mining of which has resulted in exceptional exposures (Fig. 10). Qt4–5 deposits typically exhibit a coarsening-up progression (Calderoni et al., 1991) from a basal meandering channel facies to a braided channel facies. Locally, a capping meandering channel facies occurs in the upper few meters of the Qt4–5 deposit (Fig. 4). In several locations, stratified hillslope deposits directly interfinger with Qt4–5 axial channel gravels. The Qt4–5 tread soil is brown (Munsell 7.5 YR 4/3), calcic, and not as thick as the Qt3 soil.

The Qt4–5 strath outcrops in eight localities along the Musone River. Downstream of valley km 25 the Musone is an alluvial channel with no exposed bedrock. Here, the Qt4–5 strath dives beneath the elevation of the modern Musone floodplain (Fig. 11), and the tread is eventually buried by Holocene alluvial sediments downstream of valley km 15 (Coltorti, 1996; Nanni et al., 1996). Between Filottrano and San Vittore the Qt4 strath increases in height above the modern channel from 21 to 26 m between valley km 28 and 36.5 (Fig. 11). At the mouth of the Cingoli Gorge the Qt4–5 strath is 6 m above the modern channel; it then rises to 24 m within the confines of the gorge at valley km 42. Upstream of Cingoli Gorge, the Qt4–5 strath is either not exposed or at the same elevation as the modern channel, having been exhumed only recently by Late Holocene cut-and-fill cycles (Fig. 11).

Datable materials collected from the Qt4–5 fill correspond to places where the strath is clearly exposed (Figs. 4 and 10; Table 3). The oldest Qt4–5 fill age of 35,910 ± 330 ybp was obtained 4 m above the strath in a quarry near San Vittore (Fig. 10). Three additional dates from near the center of the same fill ranged between 31,740 ± 240 and 30,470 ± 310 ybp. At the top of the fill and within the Cingoli Gorge, an inset channel yielded a calibrated age of 19,870 ± 160 ybp (Fig. 10, Table 3). These dates are commensurate with radiocarbon ages reported from the 3rd-order terrace fills elsewhere in the Marche (Table 4); therefore we set the period of Qt4–5 strath cutting as 40 ± 5 ka (MIS 3). The burial of the strath begins at 28 ± 8 ka and continues through at least 19 ka (Tables 4 and 5).

Through the Cingoli Gorge the Musone River flows in incised meanders cut into resistant Mesozoic limestones. Within the gorge the Qt4–5 strath separates into two distinct bedrock benches, each mantled with their own alluvial cover (Qt4 and Qt5) (Figs. 10 and 11). Qt5 is particularly well exposed with 3–4 m of axial channel gravels interspersed with sandy silt lenses deposited above a nearly planar bedrock strath, the geometry of which is preserved within
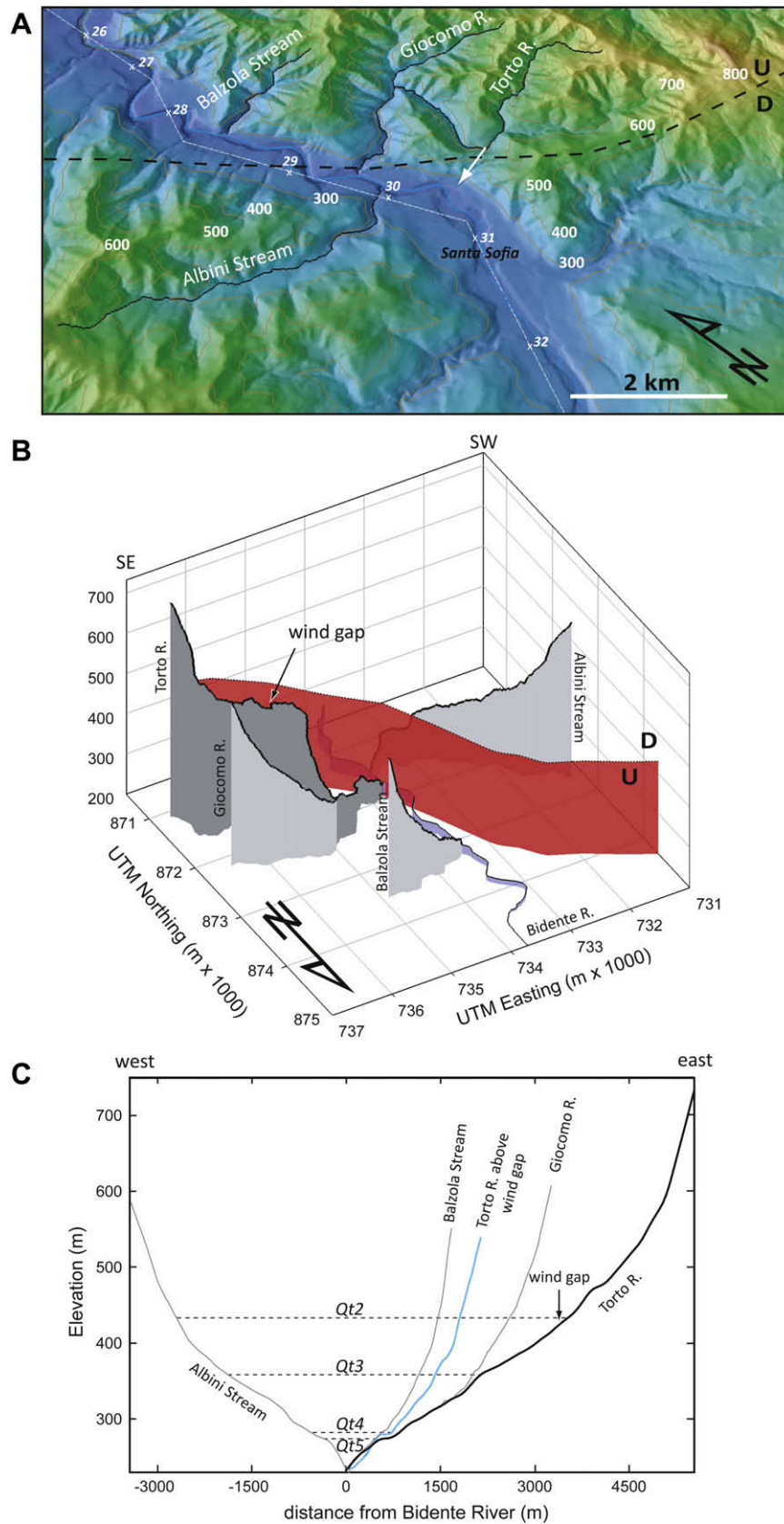
Fig. 9. Evidence for Quaternary faulting in the Bidente basin near Santa Sofia. A. Perspective DEM view to the northeast across the Bidente valley between 26 and 32.5 km showing the locations of tributary streams, the Torto River wind gap (white arrow), and inferred fault trace (dashed black line) with the north side up. B. 3-d perspective view to the southeast of tributary longitudinal profiles downstream of Santa Sofia. The prominent low slope to convex knick zone in the Torto River profile correlates to the spatial position of the wind gap and the trace of the fault. C. Tributary longitudinal profiles showing the location of the wind gap along the Torto River in comparison to the height of the Qt2 terrace. The upper portion of the Torto River longitudinal profile (blue line) above the wind gap is reproduced for comparison to the steepness of adjacent tributary stream profiles. The elevations of terrace straths (dashed horizontal lines) are coincident with knickpoints along tributary longitudinal profiles.
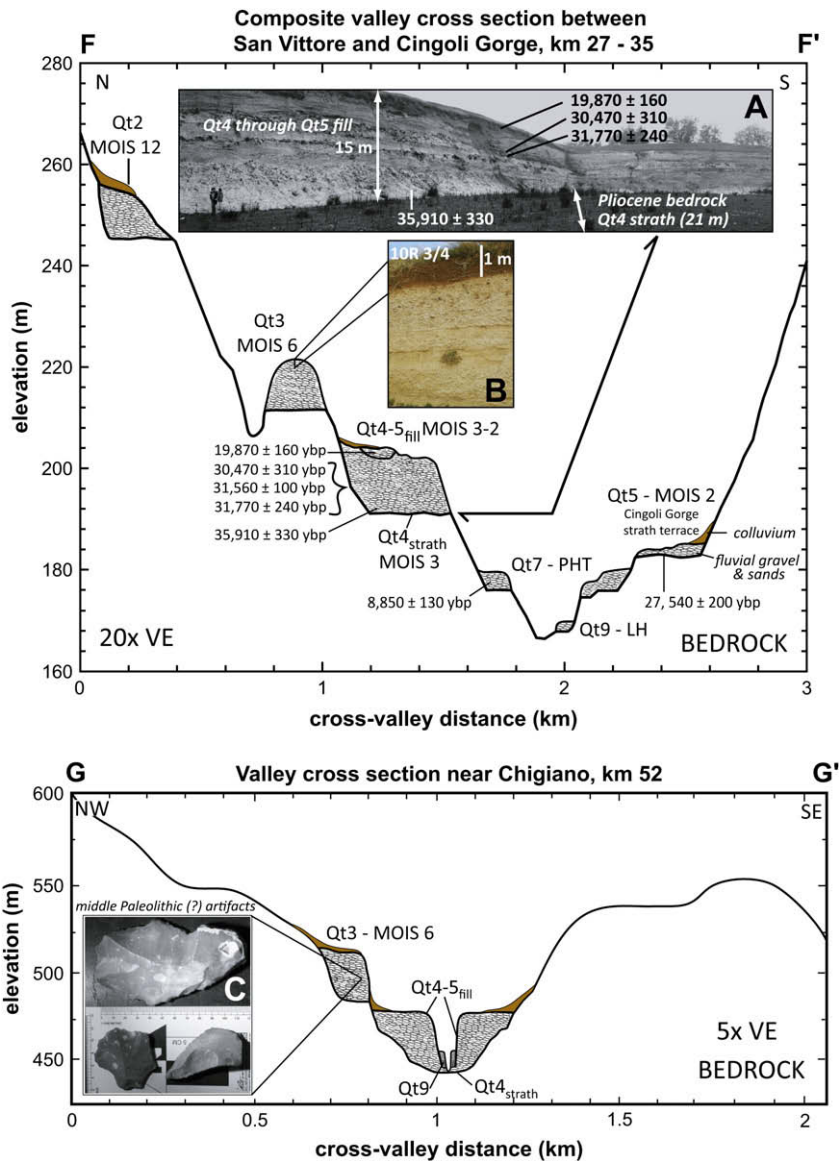
Fig. 10. Topographic profiles (F–F′ and G–G′ of Fig. 4) and composite cross-sections at two locations in the Musone River basin showing the spatial distribution of fluvial terraces and the inferred Marine Oxygen Isotope Stage (MIS) during which the strath surfaces were beveled for the San Vittore to Cingoli Gorge reach (valley km 27–35) and near Chigiano (valley km 52). The Pleistocene terraces are all fills, with deposits up to 15 m thick. The Holocene terraces are thin fills to straths. Top: overall distribution and nomenclature for the terraces within the Musone basin. The terraces in this section of the river exhibit strath separation. Inset Photo A: abandoned quarry high-wall exposure of fill sediments above the Qt4 strath cut across Pliocene mudstones (note people for scale). ¹⁴C dating confirms that the fill deposits spans the Qt4–5 interval. Inset Photo B: Dusky Red (Munsell 10R 3/4) soil with a meter thick B-horizon developed in the limestone gravel parent material of Qt3. Bottom: spatial relationship between the Qt3 and Qt4–5 fill terraces in the Chigiano reach, showing less evidence of strath separation. Inset Photo C: stone tool artifacts collected in place from an exposure of Qt3 gravels near Chigiano. Artifacts exhibit similarities to lithic tools attributed to an early facies of the Levallois Mousterian period of the Middle Paleolithic. Artifacts such as these support the assignment of Qt3 deposits to >100 ka, consistent with an MIS 6 designation.

tight meanders. The Qt5 strath at valley km 42.4 is 14 m above the modern channel, whereas the Qt4 strath 300 m downstream is 24 m (Data Repository DR-2). A calibrated radiocarbon date from the Cingoli Gorge Qt5 yielded an age of $27,540 \pm 200$ ybp, constraining the timing of Qt5 strath formation by lateral channel widening to the beginning of MIS 2 (Tables 3 and 5).

The Pleistocene-to-Holocene transitional (Qt6) and Middle Holocene (Qt8) terraces, so prominent in the Bidente basin, are not represented in the Musone terrace sequence. Instead, only Holocene terraces Qt7 and Qt9 in the Musone basin are inset into the Late Pleistocene Qt4–5 valley (Fig. 10) and are predominantly of the fill-cut variety, the straths of which are seldom exposed. However, between Filottrano and San Vittore two separate Holocene strath terraces corresponding to Qt7 and Qt9 are observed (Figs. 4 and 10).

Both upstream and downstream of this reach, Qt7 and Qt9 transition back into fill terraces ($\sim$10 m thick). The Qt7 strath, identified in three localities, increases in height across a distance of 0.5 km from 0 to 10 m above the modern channel at valley km 30 to a maximum of 12 m at valley km 34.8 (Fig. 10; Data Repository DR-2). The Qt9 bedrock strath, 3.5 m above the modern channel, is exposed along a 1 km reach centered on valley km 36.5 (Fig. 5C).

Deposits of the Qt7 strath terrace at San Vittore yielded a calibrated radiocarbon age of $8,850 \pm 130$ ybp. Based upon this date, the age of Qt7 strath formation is considered to be 10 ± 1 ka with the timing of fill deposition at 8.5 ± 1 ka, corresponding to a period of valley widening and minor aggradation during the Pleistocene-to-Holocene transition (Figs. 10 and 11; Tables 3 and 5). The Qt9 strath terrace at valley km 36.5 was not dated; however, based
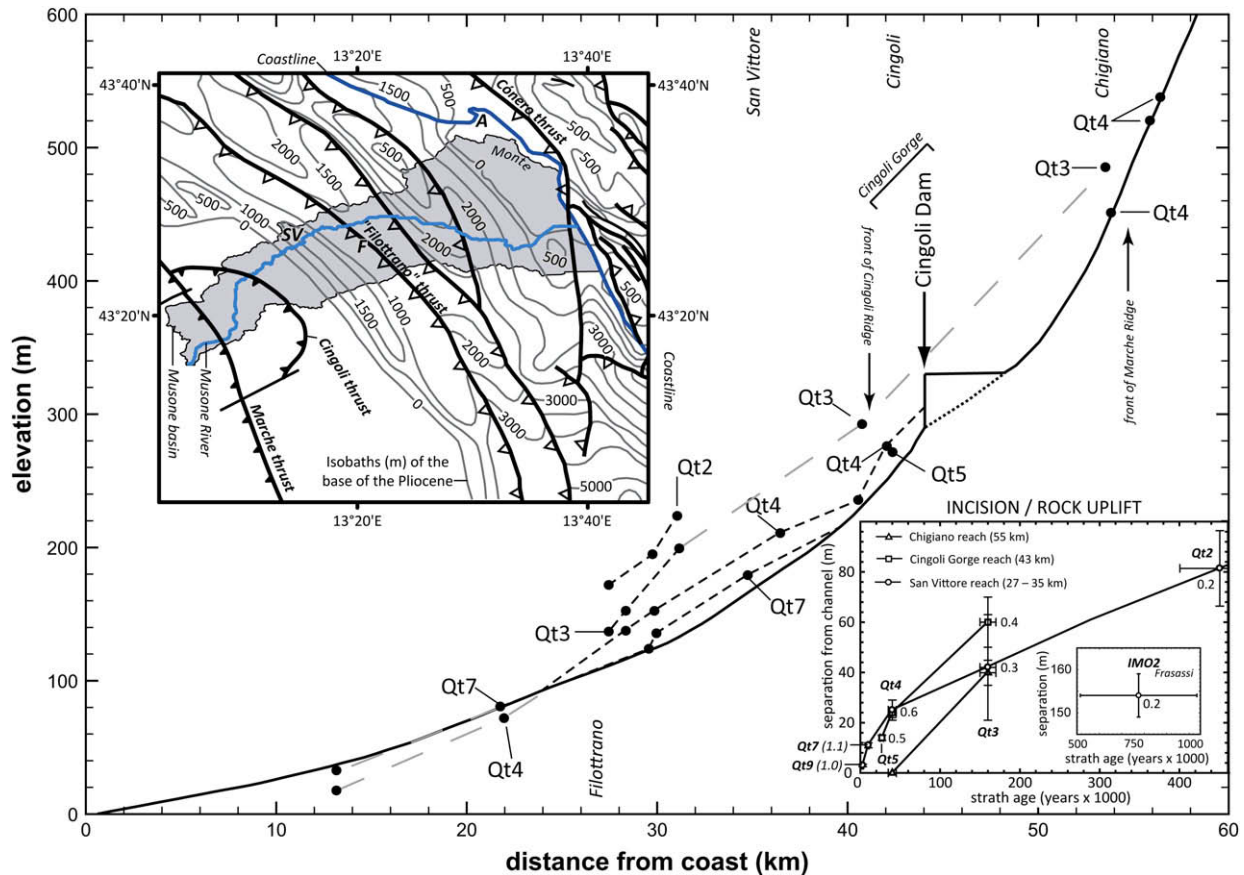
Fig. 11. Projection and correlation of reconstructed Musone River terrace strath surfaces compared to the modern Musone longitudinal profile (solid black line) showing evidence for upstream convergence near Chigiano and downstream divergence to convergence between San Vittore and Filottrano. Solid circles along the profiles indicate locations of measured bedrock strath elevations projected to the modern longitudinal profile. The lower inset diagram shows incision rates (rock uplift) between 27–35, 43, and 55 km from the Adriatic coast, with incision rates in mm/yr. The upper inset diagram is a contour map of the depth from the surface to the base of the Pliocene in the Musone basin area (shaded polygon) (Bigi et al., 1992). The heavy black lines are thrust faults with the teeth on the upthrown side. Open teeth represent buried Post-Tortonian thrust faults; filled teeth represent exposed faults at the front of the Cingoli and Marche Ridge anticlines. Note the spatial correspondence between the hinterland-most buried thrust fault and shallow depths to the basal Pliocene near the town of Filottrano (F) and the separation of Musone terrace straths in the San Vittore (SV) to Filottrano reach.

upon landscape position, geoarcheology (Coltorti, 1997), and lack of any appreciable soil it is assigned to a Late Holocene age (Table 5).

5.2.2. Terrace longitudinal profiles and incision rates

Upstream of Cingoli Gorge, the Musone River has not incised into bedrock since the formation of the Qt4 strath, as there is no separation between it and the modern channel (Fig. 11). In contrast, the terrace profiles diverge away from the modern channel in the Filottrano to San Vittore reach (Fig. 11). It is in this reach only that Qt2, the oldest and highest terrace, is preserved. Predictably, the rates of incision are greatest for this section reaching ~0.2 mm/yr, a comparable rate to what is reported for Sentino River incision of the Frasassi Gorge over the past 0.75 ± 0.26 Ma (Cyr and Granger, 2008) (Figs. 4 and 11; Table 5). In comparison, incision rates derived from the Qt3 (160 ± 10 ka) strath are 0.3 mm/yr in both the San Vittore and Chigiano reaches and a somewhat faster 0.4 mm/yr within the Cingoli Gorge. Over the past 40 ± 5 ka (Qt4), bedrock incision has proceeded at 0.6 mm/yr across the San Vittore and Cingoli Gorge reaches whereas at the front of the Marche Ridge at Chigiano it is ~0 mm/yr. Incision within Cingoli Gorge since Qt5 time (27 ± 2 ka) has averaged 0.5 mm/yr. Holocene incision rates derived from the Qt7 and Qt9 strath terraces in the San Vittore reach are ~1 mm/yr (Fig. 11, Table 5). Collectively, the data from the Filottrano to San Vittore reach suggest that bedrock incision

rates accelerated between 450 ± 50 ka (Qt2) and 160 ± 10 ka (Qt3), and the acceleration has continued into the Late Pleistocene.

6. Discussion

6.1. Geologically modulated and climatically paced terrace genesis

The predominance of either siliciclastic or carbonate bedrock cropping out in the drainage basins of the northern Apennines defines the amplitude of the geomorphic response (modulation) to periodic climate change (pacing) that collectively control terrace genesis. Basins underlain predominantly by siliciclastics and Ligurian units such as the Bidente tend to develop and preserve strath terraces, whereas basins underlain by carbonates, particularly in their middle-to-upper reaches such as the Musone, develop and preserve fill terraces. There is little doubt that rivers respond to climatically driven variations in sediment and water discharge, ultimately leading to terrace preservation in the northern Apennines and elsewhere (e.g. Nesci and Savelli, 1990; Antoine et al., 2000; Cordier et al., 2006; Bridgland and Westaway, 2008; Wegmann, 2008). What is of interest in the northern Apennines is how climate change is linked through bedrock geology and the hillslope–fluvial system to the timing of strath surface formation

Table 4
Numeric ages from Late Quaternary fluvial deposits of the Romagna and Marche Apennines.

Sample ID[a]	Lat (°N)	Long (°E)	Material[b]	δ¹³C (‰)	¹⁴C age (years)	Calibrated 1σ max[c] (yr BP)	Calibrated 1σ min[c] (yr BP)	Original terrace name[d]	Proposed terrace name	Basin[e]	Source[f, g]
AA54506	44.453	11.276	C	−26.30	1150 ± 30	1100	1010	Qt9	Qt9	R	2
AA54513	44.453	11.276	C	−27.52	1150 ± 40	1110	1000	Qt9	Qt9	R	2
AA54505	44.453	11.276	S	−9.45	1950 ± 40	1930	1860	Qt9	Qt9	R	2
Beta-87660	43.04	13.46	C	n/a	3570 ± 70	3960	3770	4°	Qt8	T	3
n/a	43.36	13.50	C	n/a	4680 ± 100	5550	5290	4°	Qt8	P	5
AA61344	44.401	11.261	C	−26.04	5330 ± 40	6200	6040	Qt8	Qt8	R	2
AA61346	44.401	11.261	C	−25.54	5630 ± 40	6450	6360	Qt8	Qt8	R	2
Rome-508	43.31	13.39	C	n/a	7210 ± 90	8100	7950	4°	Qt7	P	5
Beta-87661	43.04	13.46	C	n/a	7620 ± 80	8480	8350	4°	Qt7	T	3
AA64963	43.439	13.248	S	−6.8	7970 ± 50	8980	8730	4°	Qt7	M	1
n/a	n/a	n/a	T	n/a	8260 ± 100	9400	9100	4°	Qt7	E	3
AA64959	43.976	11.908	S	−6.9	8700 ± 70	9760	9550	Qtb3b	Qt7	B	1
AA64285	44.338	11.214	C	−24.90	9560 ± 60	11,030	10,740	Qt6	Qt6	R	2
AA64287	44.358	11.211	S	−7.70	9920 ± 60	11,390	11,220	Qt6	Qt6	R	2
AA64286	44.338	11.214	S	−8.60	10,410 ± 60	12,470	12,180	Qt6	Qt6	R	2
AA65341	44.030	11.982	S	−6.5	10,600 ± 60	12,650	12,540	Qtb3a	Qt6	B	1
AA64284	44.338	11.214	S	−7.80	10,700 ± 80	12,730	12,590	Qt6	Qt6	R	2
AA64966	44.000	11.935	S	−6.9	11,090 ± 70	13,130	12,900	Qtb3a	Qt6	B	1
AA65342	43.910	12.123	S	−6.7	11,100 ± 60	13,130	12,920	Qtb3a	Qt6	S	1
AA54512	44.436	11.266	C	−22.52	12,690 ± 50	15,060	14,860	Qt6	Qt6	R	2
n/a	43.28	12.99	C	n/a	14,700 ± 150	18,200	17,680	3°	Qt4–5	E	6
n/a	43.28	12.99	C	n/a	15,250 ± 160	18,710	18,430	3°	Qt4–5	E	6
AA64961	43.392	13.183	S	−4.7	16,730 ± 90	20,030	19,700	3°	Qt4–5	M	1
AA65340	44.130	12.074	S	−5.8	18,870 ± 140	22,560	22,330	Qtb4	Qt5	B	1
AA65340r	44.130	12.074	S	−5.8	19,180 ± 130	23,000	22,570	Qtb4	Qt5	B	1
AA61345	44.341	11.200	S	−6.61	19,320 ± 120	23,270	22,760	Qt5	Qt5	R	2
AA54503	11.426	11.264	S	−6.80	19,670 ± 90	23,700	23,490	Qt5	Qt5	R	2
Beta-87662	43.31	13.39	C	n/a	20,020 ± 150	24,150	23,810	3°	Qt4–5	T	3
AA64964	43.392	13.178	S	−7.1	23,020 ± 170	27,730	27,340	3°	Qt5	M	1
n/a	43.30	12.98	W	n/a	23,500 ± 400	28,470	27,610	3°	Qt4–5	E	4
AA65339	44.091	12.086	S	−4.7	23,840 ± 320	28,750	28,050	Qtb5	Qt4	B	1
AA64965	43.458	13.299	S	−9.3	>24,800	n/a	>28,570	3°	Qt4–5	M	1
AA65338	43.428	13.233	S	−7.5	25,260 ± 210	30,780	30,160	3°	Qt4–5	M	1
UCI21619	43.458	13.299	S	−2.9	26,540 ± 90	31,650	31,460	3°	Qt4–5	M	1
Rome-242	43.09	13.12	W	n/a	26,800 ± 700	32,860	31,320	3°	Qt4–5	Ch	7
AA646962	43.428	13.233	W	−28.1	26,810 ± 290	32,020	31,530	3°	Qt4–5	M	1
Rome-242a	43.09	13.12	W	n/a	30,150 ± 1200	36,740	34,340	3°	Qt4–5	Ch	7
n/a	43.30	12.98	W	n/a	30,200 ± 900	36,110	34,280	3°	Qt4–5	E	4
UCI21620	43.428	13.233	C	−22.5	30,980 ± 240	36,240	35,580	3°	Qt4–5	M	1
Rome-111	43.59	12.94	W	n/a	31,700 ± 1050	37,710	35,570	3°	Qt4–5	Ce	4
n/a	43.27	13.00	W	n/a	31,800 ± 1100	37,870	35,620	3°	Qt4–5	E	4
n/a	n/a	n/a	W	n/a	31,920 ± 1030	37,930	35,790	3°	Qt4–5	Co	8
Rome-110	43.65	12.99	W	n/a	32,500 ± 1200	38,790	36,140	3°	Qt4–5	Ce	4
n/a	43.30	12.98	W	n/a	32,500 ± 1200	38,790	36,140	3°	Qt4–5	E	4
n/a	43.32	12.98	W	n/a	32,700 ± 1200	39,030	36,330	3°	Qt4–5	E	4
n/a	n/a	n/a	W	n/a	34,760 ± 1505	41,580	38,340	3°	Qt4–5	Co	8
Rome-108	43.65	13.00	W	n/a	35,600 ± 1800	42,420	39,010	3°	Qt4–5	Ce	4
Rome-109	43.65	13.00	W	n/a	37,300 ± 2200	43,900	40,280	3°	Qt4–5	Ce	4
Rome-112	43.59	12.94	W	n/a	37,300 ± 2200	43,900	40,280	3°	Qt4–5	Ce	4
n/a	43.28	12.99	W	n/a	41,400 ± 4000	48,900	40,900	3°	Qt4–5	E	4
n/a	n/a	n/a	n/a	n/a	42,000 ± 4000	49,690	41,690	3°	Qt4–5	Ce	9

[a] Samples beginning with (AA) were analyzed at the University of Arizona Accelerator Mass Spectrometry Laboratory; (Beta) were analyzed at Beta Analytic, Inc.; (Rome) were analyzed at the University of Rome Radiocarbon Lab; (UCI) were analyzed at the University of California Irvine W.M. Keck Carbon Cycle Accelerator Mass Spectrometry Laboratory.

[b] Type of organic material dated: C = charcoal, S = shells, T = travertine, W = wood.

[c] All ages were calibrated using the Fairbanks0805 radiocarbon calibration curve (Fairbanks et al., 2005).

[d] The degree symbol (°) is shorthand notation for terrace order; fill terraces from the Marche traditionally have been assigned 1st through 4th-order, depending upon their height and inferred age above the modern channel.

[e] Basin abbreviations are: B = Bidente, Ce = Cesano, Ch = Chienti, Co = Conca, E = Esino, M = Musone, P = Potenza, R = Reno, S = Savio, T = Tenna (Figs. 3 and 4).

[f] Source of data: 1 = this study, 2 = Eppes et al. (2008), 3 = Cilla et al. (1996), 4 = Calderoni et al. (1991), 5 = Calderoni et al. (1996), 6. = Alessio et al. (1979), 7 = Damiani and Moretti (1968), 8 = Forlani (1987), and 9 = Nesci et al. (1995).

[g] Ages are only reported if there is sufficient stratigraphic control to insure that the samples were collected from immediately above the bedrock strath for strath terrace deposits of the Emilia–Romagna Apennines and from the fill terrace deposits of the Marche Apennines. Reported ages from soils and colluvial deposits developed on the treads of fluvial terraces (e.g. Amorosi et al., 1996) are not included.

and the style of terrace preserved within the two types of basins (Fig. 12).

Results based on the numeric ages of terrace deposits from the Bidente, Reno and Savio River basins (Fig. 13A; Table 4) correspond to times of maximum Northern Hemisphere ice volume indicating that periods of valley widening and strath formation immediately preceded the coldest and driest climatic conditions. Apparently, wide straths are carved when the climate of the Romagna Apennines is changing from relatively warm and humid (interglacials and/or interstadials) to cool and dry (glacial and/or stadials). We

Table 5
Musone terrace ages and incision rates.

Terrace	strath age (ka)	aggradation age (ka)	MIS[a]	Height[b] of Strath above channel (m)	incision rate[b] (mm/yr)	Source
Qt9	3 ± 1	2 ± 1	1	3 ± 0.5	1.0 ± 0.1	Soil chronostratigraphy; Eppes et al. (2008)
Qt7	10 ± 1	8.5 ± 1	1	11 ± 1	1.1 ± 0.02	[14]C, This study
Qt5[c]	27 ± 2	23 ± 5	2	14 ± 1	0.5 ± 0.003	[14]C, This study
Qt4–5[d]	40 ± 5	28 ± 8	3–2	25 ± 4	0.6 ± 0.02	[14]C, This study
Qt3	160 ± 10	140 ± 10	6	42 ± 22	0.3 ± 0.02	Taddeucci et al. (1992)
Qt2	450 ± 50	440 ± 50	12–10	73 ± 15	0.2 ± 0.002	MIS
IMO 2[e]	775 ± 260	775 ± 260	19	154 ± 5	0.2 ± 0.004	[26]Al:[10]Be burial age (Cyr and Granger, 2008)[e]

[a] MIS = Marine Isotope Stage.
[b] Strath elevations and river incision rates, except for Qt5 (Cingoli Gorge) and IMO 2, are averages for terraces in the San Vittore reach (valley km 27–35).
[c] Exists as a strath terrace only within the Cingoli Gorge.
[d] The strath was cut during the Qt4 interval; the fill above the strath represents aggradation during the Qt4 (MIS 3) and Qt5 (MIS 2) intervals.
[e] Cosmogenic nuclide [26]Al:[10]Be burial age for sediments in Grotta della Madonna – Frasassi Gorge, probable continental equivalents to IMO 2 (Sabbie Gialle) coastal deposits (Cyr and Granger, 2008).

suggest that the cooling and drying of Romagna climate destabilizes hillslope soils and colluvium, previously held in place by continuous vegetative cover. Frost fracturing of exposed bedrock likely contributes to colluvial sediment yields during cold intervals (Coltorti and Dramis, 1995; Veldkamp and van Dijke, 2000). The strath surfaces are at their widest and mantled by a thin mobile alluvial layer during peak glacial periods. In our model, straths are preserved as terraces by the ensuing channel incision and floodplain narrowing as the climate warms into the subsequent interglacial. This model is supported by radiocarbon evidence (Figs. 6, 12 and 13; Table 4) and observable stratigraphic relationships clearly showing a Holocene valley (Qt6–Qt9) inset into the MIS 2 valley of Qt5, which in turn is inset into the MIS 6 valley of Qt3 (Fig. 6). These observations contrast with studies from northwestern European rivers (e.g. Antoine et al., 2007), where there is evidence for vertical river incision occurring at the time of warm-to-cold climatic transitions and may indicate differences in how accommodation space (incision) is created in relatively stable northwestern Europe and tectonically active Italy.

The Romagna landscape is currently being lowered at 200–400 m/m.y. (Cyr and Granger, 2008), a rate representative for the Holocene. Anthropogenic effects aside, the sediment flux being delivered to the channel by these erosion rates must be less than the Late Pleistocene rates because the width of the Holocene valley is narrower, and fully contained within the Late Pleistocene valley. The magnitude of the sediment flux difference is difficult to know, but we surmise that it is primarily responsible for the difference in the wide Late Pleistocene strath with respect to the narrower Holocene strath.

Gravel bed mining activities over the past 50 years provides a timely natural experiment illustrating the effects of variable bedload on channel erosion properties (Brugnara and Zannoner, 1997). Apparently the Bidente and other Emilia–Romagna streams were at or near capacity throughout the Holocene as small changes in climate or land use resulted in the construction or incision of a floodplain that was more or less in contact with the channel. Recent and nearly complete anthropogenic removal of the gravel and sand bedload of these channels has resulted in incision, sometimes dramatic, as the bedrock floors of these channels have lowered 2–12 m below their floodplains. The pre-mining condition mimics a glacial period for Romagna streams when there was ample delivery of weathered Marnoso Arenacea Fm gravel and sand to channels that were able to carve a wide (Holocene) strath, while still maintaining a transport gradient sufficient to move all of the bedload downstream. The post-mining condition mimics a cold-to-warm transition into an interglacial (interstadial), when the channel is abruptly starved of sediment as a warming climate and vegetation stabilize contributory hillslopes. The exposed channel rapidly incises, forming a terrace out of its former floodplain, as it seeks a lower transport gradient in balance with the underlying rock type and diminished bedload.

We appeal to a similar general model for the production of fill terraces in the Musone basin with the difference being attributed to a much greater volume of weathered carbonate detritus delivered to the channel bedload. During full-glacial climatic conditions carbonate ridges lacking vegetation were subjected to intense periglacial weathering (Coltorti and Dramis, 1995). This periglacial weathering produced copious amounts of centimeter-sized, angular micritic and marly limestone flakes for as long as the cold conditions persisted (Nesci and Savelli, 1990; Calderoni et al., 1991), thick remnants of which remain as stratified slope-waste (grèze litée) deposits (Coltorti and Dramis, 1995). The consequence of all this sediment coupled with diminished discharge forced Marche streams past the point of carving wide straths to storing alluvium in the valley (Fig. 12). A steepened transport gradient was required to move the alluvium under drier conditions, leading to thick alluvial fills with foreland-dipping treads characteristic of the Musone and other Marche rivers.

Qt4 and Qt5 nicely illustrate differences between Bidente and Musone terrace genesis. In the Bidente basin, Qt4 and Qt5 define two distinct landforms and two distinct periods of strath cutting and burial at ∼35 ka and ∼20 ka, respectively. The Musone basin, in contrast, contains one thick fill sequence, Qt4–5 that spans roughly the same time interval and buries only one strath for most of the basin (Figs. 10, 12 and 13C; Table 4).

The numeric ages also indicate, however, that the straths underlying terraces in the Musone basin are older than their Bidente counterparts (Tables 3 and 5). The Bidente channel remains in contact with bedrock throughout the cold interval as the thin (≤3 m) axial channel deposits above the strath were continuously mobilized and reworked downstream during higher discharges. In contrast, the Musone channel quickly abandons it strath and begins aggrading at the onset of a cold climate as large amounts of carbonate detritus overwhelm its sediment transport capacity. In this respect the time interval represented by aggradation in the carbonate basins is the same time interval represented by wide strath carving in basins underlain by siliciclastics. In contrast, channel incision and terrace formation in both basin types are approximately in phase and during the cold-to-warm climatic transitions (Figs. 10, 12 and 13; Table 4), although incision rates may be initially faster for carbonate basins as they have a greater amount of fill to incise and the channel has been insulated from its bedrock floor for a longer period of time (Fig. 12).

The general terrace chronostratigraphy of the Bidente and Musone Rivers shares similarities to chronologies developed for other well-studied rivers in mainland Europe and the Iberian Peninsula (Fig. 7). For example, the terrace record from the Maas
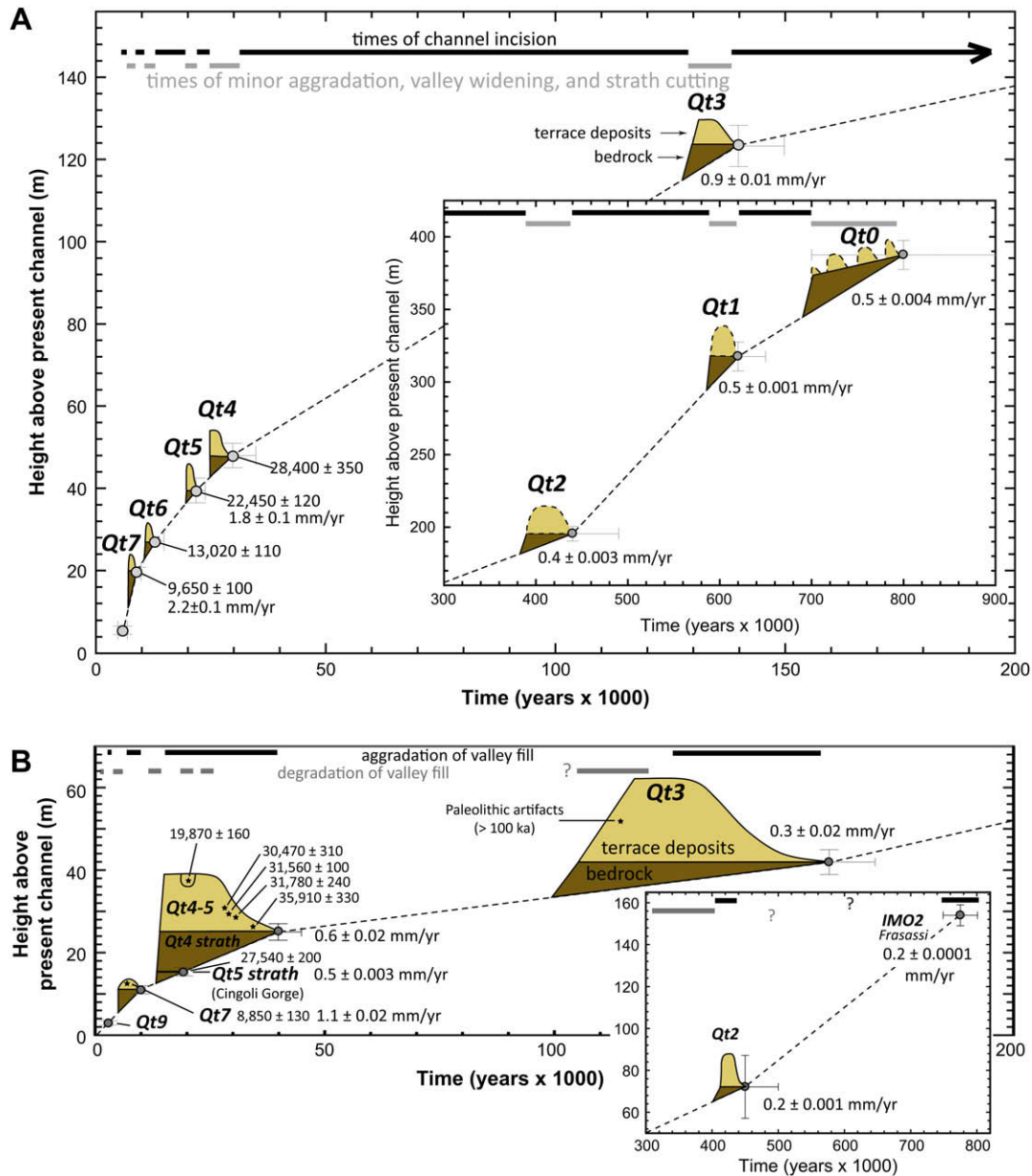
Fig. 12. Summary diagrams of combined influence of tectonic and climatic controls on the Late Quaternary behaviors of the (A) Bidente and (B) Musone Rivers as reflected by changes in streambed altitude. Calibrated ^{14}C ages and incision rates in mm/yr are shown for each terrace (Tables 3 and 5).

River of the Netherlands has been argued to record fluvial system response to ∼100 ka orbitally forced glacial cycles (e.g. van den Berg and van Hoof, 2001; Westaway, 2001; Bogaart et al., 2003b; Bridgland and Westaway, 2008) similar to what we observe for the Bidente (Fig. 7). With higher fidelity, the record from the Guadolope River in Spain's Ebro basin (e.g. Fuller et al., 1998; Santisteban and Schulte, 2007) mimics the Marche aggradation–incision record (Fig. 13C) over the Late Pleistocene to Holocene. Both the Marche and Guadolope sequences appear to preserve evidence for basin aggradational episodes that coincide with stadial or Holocene neoglacial events, whereas phases of river incision occur during interstadial or interglacial periods (Fig. 13C), likely in response to changes in hillslope vegetation, periglacial weathering processes and the seasonality and intensity of precipitation events. The similarities between the Maas and Ebro records and the Apennine terrace chronostratigraphy support the notion of teleconnections between hemispheric climate changes and localized drainage basin response.

6.2. River incision as an indicator of active shortening

The terrace record clearly indicates that both the Bidente and Musone Rivers have incised into bedrock, including along their lower reaches, since at least the Middle Pleistocene. The incision has been both non-uniform and unsteady, an observation consistent with continued shortening and active deformation in the Romagna and Marche Apennine foreland. For example, the Bidente River incision can be explained by the Apennines tilting towards the foreland (e.g. Zattin et al., 2002) with localized deformation above the proposed Pedeapenninic thrust (Fig. 1; Boccaletti et al., 2004), and normal fault-offset terraces near the drainage divide (Figs. 8 and 9). Similarly, the Musone contains evidence of fold and/ or thrust tectonic activity in the San Vittore region above the shallow, blind "Filottrano thrust" (Fig. 11). We recognize that fluvial adjustments to Pleistocene climates have been documented to lower overall channel gradients through incision (Dethier, 2001),
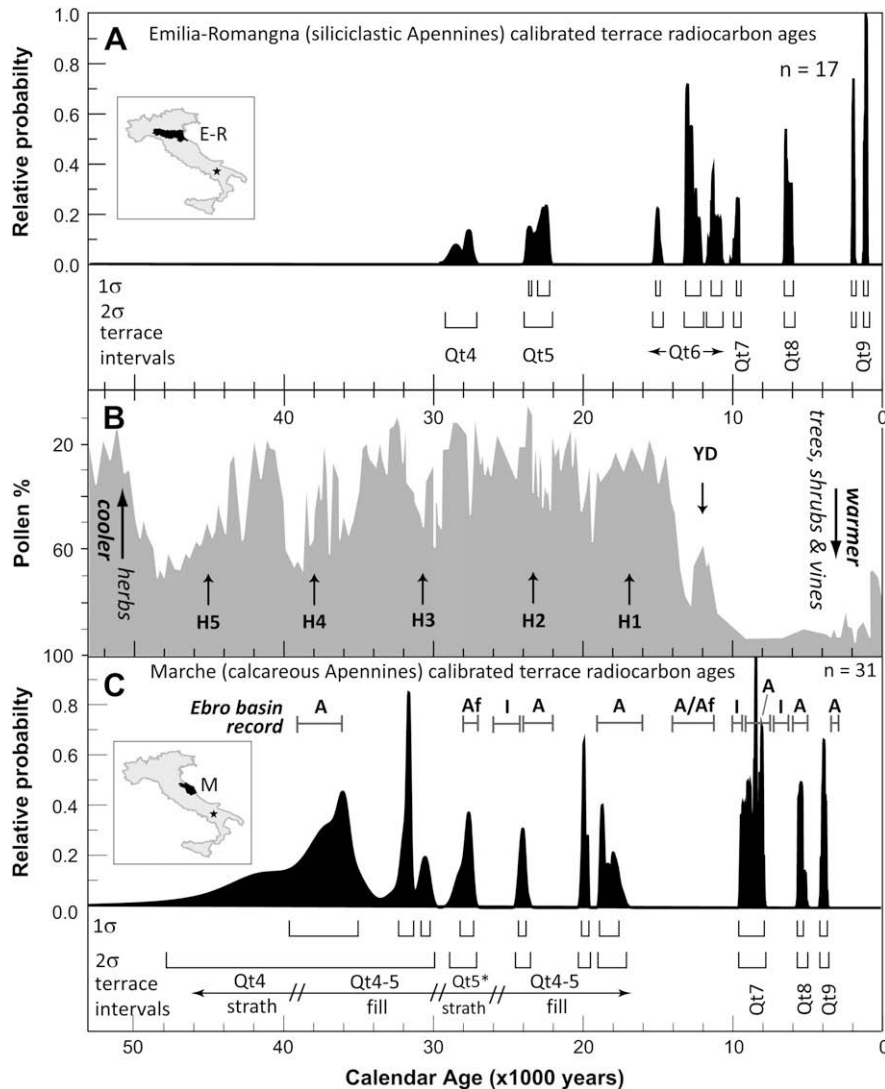
Fig. 13. Compilation of stratigraphically reliable radiocarbon ages from the literature for fluvial terrace deposits in the Emilia–Romagna and Marche Apennines (Table 4). A. Probability density plot for 17 ^{14}C analyses (Table 4) from terrace deposits in the Bidente, Reno and Savio Rivers, which drain areas underlain predominantly by siliciclastic rocks (Fig. 2). The plot was produced by calculating calendar ages and their accompanying 1σ errors with the Fairbanks0805 radiocarbon calibration curve (Fairbanks et al., 2005) and then summing the probabilities using the OxCal Program v. 3.10 (Ramsay, 2005). Note the 1 and 2σ brackets and the assigned terrace intervals beneath the frequency histograms. B. Percentage pollen diagram for trees, shrubs and vines (white) vs. herb pollen (gray) from a lacustrine record retrieved from Lago Grande di Monticchio, southern Italy (Watts et al., 2000) used as a proxy for intervals of warmer and cooler climate on the Italian Peninsula. The location of Lago Monticchio (star) relative to the Emilia–Romagna (E–R) and Marche (M) regions, respectively, is shown on the inset maps of Italy above and below the pollen diagram. The stratigraphic position of the Younger Dryas (YD) and Heinrich (H) events 1–5 is from Hemming (2004). Heinrich events tend to precede a return to cold and dry conditions as recorded in the Lago Monticchio pollen record. C. Probability density diagram of 31 ^{14}C analyses from terrace deposits from seven river basins in the Marche region (Table 4). All of these rivers drain a mixture of calcareous and siliciclastic rocks, but the fluvial sedimentology of the deposits is dominated by the calcareous component. Note that the Qt5 strath is only identified in the Cingoli Gorge section of the Musone basin; elsewhere the Qt4–5 terrace fill is a continuous depositional unit on top of a Qt4 strath surface. Intervals of valley (A) and alluvial fan (Af) aggradation and valley incision (I) from Late Pleistocene-to-Holocene fill terraces from the Guadalope River basin (Fuller et al., 1998), a sub-basin of the larger Ebro basin in Spain, are shown for comparative purposes to the ^{14}C chronology of valley filling and incision as preserved in the relative probability distribution from the seven Marche rivers.

but we are struck by the incision patterns of the two streams we studied because so much of it has occurred near sea level and is incongruent with incision patterns from directly adjacent reaches. These observations, plus the numerous studies that do not document differential incision (e.g. Di Bucci et al., 2003; Mayer et al., 2003; Borraccini et al., 2004) from adjacent Apennine basins, compel us to explore possible tectonic mechanisms.

The rate of river incision has not been steady but rather nearly doubles between Qt2 (~450 ka) and Qt3 (~150 ka) time in the widely spaced Reno (Picotti and Pazzaglia, 2008), Bidente and Musone basins, and continued to accelerate after Qt3 (Figs. 8 and 11). We recognize that rates averaged over short timescales are typically faster than long-term rates (Gardner et al., 1987; Wegmann and Pazzaglia, 2002) and that there have been significant

anthropogenic contributions to recent channel entrenchment, but the acceleration in incision is a phenomenon that begins before Qt3 time suggesting a response to accelerated base level fall (rock uplift). Furthermore, subsidence of the Po Plain in front of the Bidente basin similarly increases at ~150 ka (Di Dio, 1998; Amorosi et al., 2004), consistent with a deformation process translating rocks vertically with respect to regional. One possibility is that shortening attributed to the continued subduction of Adria is being concentrated or localized on a single, master deep crustal thrust (the Pedeapenninic thrust) that is responsible for the emergence and accelerated growth of the Apennine mountain front since the Early Pleistocene (Picotti and Pazzaglia, 2008).

We document three clear examples of non-uniform incision in the two studied basins, each one best explained by a local tectonic

mechanism tied to the broader geodynamic processes building the Apennines. The first example is in the headwaters of the Bidente basin near the town of Santa Sofia where offset older terraces (Qt1 and Qt2) and upstream convergence of Qt4–Qt8 profiles along the same reach are best explained by offset astride high-angle normal faults (Figs. 8 and 9). One explanation for the normal-sense offsets on these terraces is that they are marking the latest Quaternary position of the extensional deformation front across the Apennine topographic divide. A NW–SE striking fault just north of Santa Sofia that offsets the Qt1–Qt2 straths has been recognized via regional mapping as either a northeast vergent south-dipping thrust (Agenzia per la protezione dell'ambiente e per i servizi tecnici, 2007) (Fig. 2A), or as part of the southwest verging north-dipping 'Portico back-thrust system' (Bonini, 2007). We note instead that grabens in the Tuscan extensional domain have a mean spacing of ∼30 km and show a progression from older to younger basins towards the Apennine crest. The youngest Tuscan graben (Casentino basin) lies 30 km to the south of Santa Sofia and 30 km north of the Valdarno basin, a more mature, sediment-filled depression (Figs. 1, 2A and 3A). In addition, earthquake focal mechanisms recorded near Santa Sofia and along strike to the northwest and southeast exhibit predominantly normal to normal-oblique motion (Boccaletti et al., 2004). Therefore, the faults at Santa Sofia might presage the advancement of the extensional front across the present-day Apennine topographic divide, and their initiation is constrained between Qt1 and Qt2 time. The preservation of a wind gap near the paleomouth of the Torto ('twisted') River graded to the Qt2 strath suggests that activity on the fault ∼400 ka was sufficient to instigate headward capture of the lower Torto River by a tributary of the Giocomo River (Fig. 9).

The second example occurs at the mouth of the Bidente River where the projection of the steeply dipping terraces into the Po subsurface supports the growing consensus that a significant amount of the horizontal compressional deformation across the Apennines, as revealed by recent GPS (Serpelloni et al., 2005), geodetic releveling (D'Anastasio et al., 2006), interferometry (Stramondo et al., 2007), and geomorphic analyses (Picotti and Pazzaglia, 2008), may be concentrated above a deep, active Pedeapenninic thrust (Figs. 8 and 10). Such an interpretation is consistent with recent Mw > 5 deep thrust events beneath the Emilia–Romagna mountain front (e.g. Selvaggi et al., 2001; Piccinini et al., 2006; Pondrelli et al., 2006; Fig. 1) and trishear and flexural isostatic modelling by Picotti and Pazzaglia (2008) of geometric relationships similar to those observed in this study from the Reno River terrace sequence near Bologna. The deformation of Reno terraces at the mountain front occurs at a wavelength appropriate for a deeply buried active thrust fault and is too short to be explained as a lithospheric flexure feature (Picotti and Pazzaglia, 2008).

Deformation of the Bidente strath terrace–alluvial fan profiles can be modeled using equation (3) (Fig. 14). Such an analysis predicts that slip rates will likely vary from ∼1.2 to 8 mm/yr depending upon the precise ramp angle and stratigraphic horizon considered (Fig. 14). The results indicate that there is a near doubling of modeled slip rate between 440 ka (Qt2) and 140 ka (Qt3), similar to the increase in incision and subsidence rates during this same interval. Furthermore, the amount of fault slip (2.5–3.8 mm/yr for Qt3) required to generate the observed Quaternary stratigraphic separation is consistent with the long-term (m.y.) shortening rate of ∼3 mm/yr across the northern Marche Apennines estimated from balanced structural cross-sections (Basili and Barba, 2007) (Fig. 14).

The third example involves the downstream divergence of straths between San Vittore and Filottrano in the Musone basin that is best explained by localized deformation likely associated with an active fault-related fold or blind thrust (Fig. 11) called the Filottrano thrust that is well-known from offset isobaths on the base of the

Pliocene marine section (Bigi et al., 1992) (Fig. 11). Along the 8 km reach astride the projected surface expression of the fault, the modern channel is incising into bedrock, the straths at the base of thick Qt3 alluvial fills are unusually well exposed, and the only outcrops of Qt2 in the basin are preserved. This anomalous zone of uplifted terraces and rapid channel incision is on strike with and south of the Mondaino thrust-cored anticline, interpreted by Basili and Barba (2007) as exhibiting out-of-sequence movement as recently as the Late Pleistocene. Strath profiles across the San Vittore reach show evidence for subtle, yet progressive forelimb rotations of 0.5° (Qt2), 0.3° (Qt3), and 0.2° (Qt4) that translate into 6×10^{-7} to $5 \times 10^{-6\circ}$ yr^{-1} of tilt, similar to the long-term forelimb tilt rate of other northern Marche thrust-cored folds (Basili and Barba, 2007).

Our appeal to tectonic mechanisms to explain the non-uniform and unsteady incision behavior of the Musone and Bidente Rivers is tempered by the understanding that eustatic fall can drive similar responses for coastal rivers (e.g. Pazzaglia and Gardner, 1993; Burger et al., 2001; Tornqvist et al., 2001). However, several lines of evidence lead us to reject eustatically driven base level fall as a factor in the observed spatial distribution and accelerations in river incision. First, the Adriatic shoreline during glacial maximum (e.g. MIS 2) was tens of kilometers to the southeast of the present mouth of the Musone River, and several hundred kilometers southeast of the modern Bidente River mouth. There is no bathymetric evidence for lowstand valleys incised across the exposed Adriatic shelf, although we do acknowledge that such valleys could be backfilled by sediment. Second, we have shown clear evidence for the large alluvial fans that rivers draining to the Po Plain have constructed during glacial climates and eustatic lowstands (Di Dio, 1998; Amorosi et al., 2004). Third, the lower reaches of the Bidente and Musone Rivers are on bedrock, indicating that they are at their base level of erosion and that deeply incised sediment backfilled paleovalleys do not exists in the lower reaches of either of these basins. If anything, the interactions of eustatic fall during a time of variable and unsteady discharge and sediment yield lead to a unique basin-to-basin complex response that can vary from incision to aggradation for adjacent drainage basins (Blum and Valastro, 1993), particularly in the Marche Region where the present coastline and stream mouths are more proximal to the eustatic fall. These responses will naturally affect the tread elevations (c.f. Vannoli et al., 2004), but will have little effect on the straths that we use exclusively in this paper to document the incision variability.

We are left with the conclusion that there is compelling evidence for active shortening and localized tectonic deformation in the basins we studied, but that similar deformation is not widely reported from otherwise excellent terrace studies elsewhere in the northern and central Apennine foreland. We propose several possible explanations. First, there may be a high degree of along-strike tectonic variability, such that adjacent rivers may not need to respond to the same tectonic forcing. As an example, the Musone basin happens to be situated near the center of an arcuate thrust sheet (Figs. 1 and 2B) where the rate of compressional deformation should be maximized. Other well-studied basins, such as the Metauro (e.g. Nesci and Savelli, 1990; Di Bucci et al., 2003; Mayer et al., 2003; Borraccini et al., 2004), are larger and naturally located in between arcuate thrust sheets, where strike-slip motion oriented parallel to the valley axis may supersede compressional deformation trending transverse to the valley axis. Second, it is conceivable that the Musone straths showing evidence for downstream profile divergence in the San Vittore reach are not true valley bottom straths, but instead are just the most external lateral "wings" of terraces preserved along paleovalley margins, but this ignores the fact that the channel is incised into bedrock precisely at this point and the measured Qt3 strath elevations are within 100 m of the
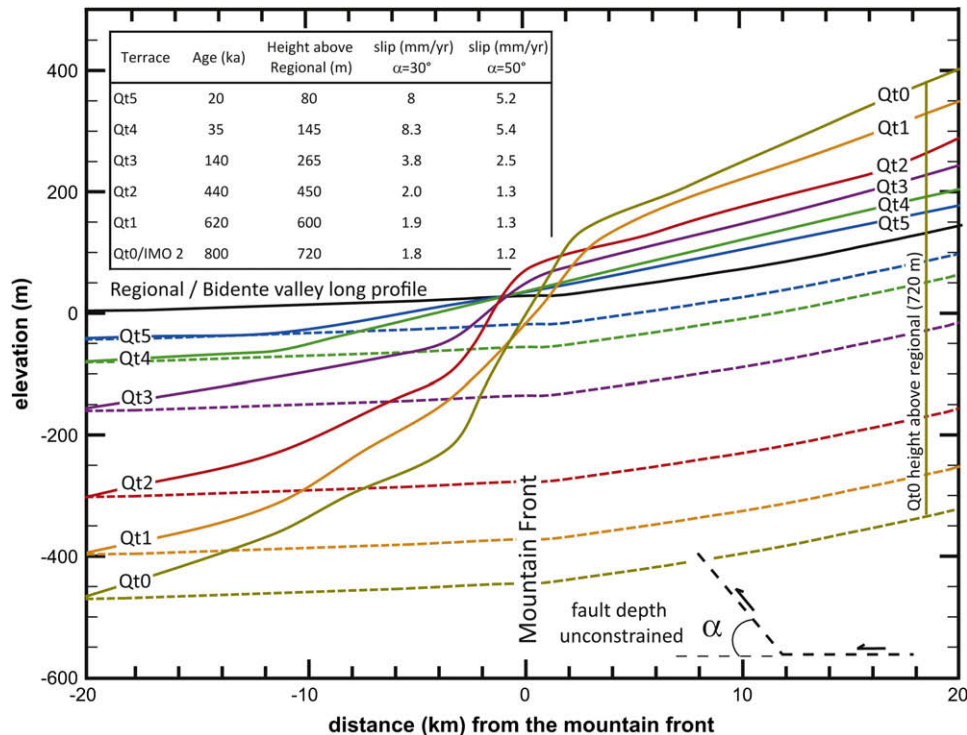
Fig. 14. Estimates of the height above regional for Bidente terrace and Po Plain subsurface deposits across a 40-km observational window centered on the mountain front, ~4 km south of Forli. The modern Bidente valley longitudinal profile (black line) is assumed to represent the long-term equilibrium valley profile (e.g. Mackin, 1948) and as such may be used as a regional datum from which the cumulative amounts of incision/uplift and subsidence for a given terrace (paired solid and dashed lines) are determined. The Height above regional can be used as a 1st-order estimate of the amount of horizontal compressive slip required along a buried thrust decollement with a ramp at a given angle (α). The inset table shows time-dependent slip rate estimates for a thrust ramp with an α of 30° and 50°; a typical thrust ramp dip, and the ramp dip determined by Picotti and Pazzaglia (2008) for a deeply buried thrust beneath the Apennine mountain front near Bologna, respectively. The analysis suggests that there is a near doubling in horizontal slip rate between 440 ka (Qt2) and 140 ka (Qt3). The slip rate estimations are likely local maximums as the analysis assumes that all of the compressive deformation across the 40-km window is accommodated on a single fault plane at depth, does not account for sediment compaction and isostatically driven subsidence of the Po Plain, or long-wavelength flexural loading.

channel. Finally, for some studies, reliance upon the elevation of treads for the reconstruction of terrace profiles, as opposed to the elevation of straths, may have resulted in misinterpretation of active tectonic deformation.

7. Conclusion

We document unsteady and non-uniform river incision in two drainages of the tectonically active northern Apennine foreland. The incision record is assembled from a new terrace chronostratigraphy, placed in the context of a broader European framework that is paced by glacial–interglacial climate change. The terrace stratigraphy provides a structure for integrating future studies within the Apennine tectono-geomorphic community around the coupling of geodynamic and earth surface processes as well as providing some 1st-order constraints for geodynamic considerations on the relative activity and growth of the Apennine wedge.

Our model for terrace genesis is supported by numeric dating, stratigraphic relationships, and correlation to the marine oxygen isotope record and appeals to a response modulated by predominant basin substrate. Intervals of wide strath carving or valley aggradation occur when hillslopes shed sediment under cold climate conditions. In basins underlain by siliciclastics, this increased sediment load drives lateral channel incision, carving wide straths in the process; however, the hillslopes remain weathering-limited, never generating and delivering large enough sediment loads to the channel network such that the river valley is periodically buried in detritus and the channel is lifted off the bedrock valley floor. In contrast, basins underlain by carbonates are

dominated by transport-limited hillslopes that generate and deliver large loads accommodated by the trunk channel through aggradation and formation of a thick, strath-burying alluvial fill. There is an early period of strath carving in these basins before transport of the sediment load becomes too great, after which processes responsible for lateral incision are replaced by vertical aggradation to steepen the transport gradient. Because of these different hydrogeomorphic responses, straths are older in carbonate basins with respect to correlative straths in siliciclastic basins. Hillslopes stabilize as they revegetate during the cold-to-warm transitions and into interglacial intervals. In response, streams are robbed of their sediment source, issuing in a phase of rapid and synchronous incision of valley fills and straths, terraces are captured in the landscape, and a new lower base level of erosion is established.

Given all of our data, the current and most parsimonious explanation for river incision rates from the Bidente and Musone basins is that incision unsteadiness over 10^3–10^5 yr timescale is climatically driven, and 10^5–10^6 yr timescales is tectonically (base level) driven. We explore the possibility that incision is driven primarily by glacio-eustatic drawdowns but ultimately reject this possibility because the Holocene channels are actively carving into bedrock in the lower elevation reaches of these rivers, precluding the presence of deeply incised eustatic lowstand valleys. Instead, incision into bedrock by these rivers was retarded during glacial times because of the larger sediment loads requiring transport. More importantly, we see evidence for localized zones of tectonic activity, including an anomalously incised reach of the Musone River, where it traverses soft mudstone coincident with the Filotrano fault, and the steep

downstream convergence and bending of the Bidente terraces at the mountain front.

Our study helps to synthesize and reconcile a large body of Quaternary geology and fluvial terrace studies conducted in the northern and central Apennines. Nevertheless, inconsistencies remain regarding why terrace profiles for all Apennine Rivers seemingly do not argue for unsteady and non-uniform incision. For these we offer the possibility that active tectonics are variable along strike and note that our interpretations originate from observations restricted to using the terrace straths, rather than the treads, as a paleogeodetic datum. Our terrace genesis model also lends credibility to the extension of numeric ages to older terraces via the marine oxygen isotope curve and makes possible more accurate incision rate calculations, a strategy perhaps not viable in the absence of a local, numerically calibrated terrace stratigraphy.

Acknowledgments

Data repository

DR-1. Geographic information for Bidente River terrace strath locations.

Id	mapped terrace name[a]	Revised terrace name (this study)	Distance from Mtn. Front (km)	River elev. (masl)[b]	Strath elev. (masl)[b]	Strath height (m)	Easting[c]	Northing[c]
1	AES 2–3[a]	Qt2	−0.20	24	65	41	750,033	895,203
2	AES 6[a]	Qt3	0.40	25	55	30	749,124	895,046
3	AES 7a[a]	Qt4	2.00	30	67	37	743,600	894,876
4	IMO 1–3[a]	Qt0	2.10	31	120	89	742,270	894,924
5	AES 6[a]	Qt3	2.20	32	77	45	742,936	894,934
6	AES 7a[a]	Qt4	3.40	35	65	30	747,344	892,606
7	AEI; AES 1[a]	Qt1	3.60	39	125	86	743,142	893,346
8	AES 8[a]	Qt8	4.80	40	44	4	745,519	891,394
9	AES 7a	Qt4	4.80	42	74	32	746,533	891,082
10	AES 6[1]	Qt3	4.80	42	95	53	746,701	891,018
11	AES 7b	Qt5	4.95	45	60	15	745,997	891,178
12	AES 2–3[a]	Qt2	5.30	44	115	71	744,445	891,089
13	IMO 1–3[a]	Qt0	5.30	45	175	130	743,076	891,586
14	AEI; AES 1[a]	Qt1	5.80	45	145	100	743,702	890,615
15	AES 6[a]	Qt3	6.80	55	125	70	744,076	889,544
16	AES 7b[a]	Qt5	6.90	56	75	19	744,978	889,375
17	IMO 1–3[a]	Qt0	7.2	32	42	10	728,119	866,964
18	AES 8	Qt8	8.10	65	70	5	745,541	888,049
19	IMO 1–3[a]	Qt0	8.30	65	225	160	742,861	888,687
20	AEI; AES 1[a]	Qt1	8.6	39	57	18	728,500	867,213
21	AES 7b	Qt5	8.70	65	90	25	744,565	887,606
22	AES 7a	Qt4	8.80	67	102	35	747,214	886,817
23	AES 8[a]	Qt6	8.90	66	80	14	744,940	887,416
24	AES 8	Qt7	9.00	70	81	11	744,903	887,292
25	AES 2–3[a]	Qt2	9.00	67	170	103	743,756	887,489
26	AEI; AES 1[a]	Qt1	9.20	67	210	143	743,419	888,090
27	AES 8	Qt8	9.30	70	74	4	744,966	886,851
28	AES 8a[a]	Qt6	10.00	70	85	15	744,339	886,496
29	AES 7b[a]	Qt5	10.00	70	97	27	743,860	886,484
30	AES 7b[a]	Qt5	11.30	82	115	33	743,930	885,225
31	AES 7a[a]	Qt4	12.00	85	125	40	743,502	884,578
32	AES 8a	Qt7	12.20	86	100	14	742,880	884,792
33	AES 8a	Qt6	12.90	95	121	26	742,724	884,125
34	AES 8a	Qt7	12.95	95	110	15	742,600	884,120
35	AES 8	Qt8	13.00	95	100	5	742,418	884,120
36	AES 6[a]	Qt3	13.00	92	175	83	743,168	883,677
37	AES 8[a]	Qt8	13.60	96	100	4	742,248	883,590
38	AES 8a[a]	Qt7	14.25	101	115	14	741,794	883,112
39	AES 8a[a]	Qt6	14.25	101	125	24	741,727	883,148
40	AES 7a[a]	Qt4	15.40	109	150	41	741,779	881,822
41	AES 8a[a]	Qt6	16.10	115	140	25	741,014	881,217
42	AES 6[1]	Qt3	16.10	115	190	75	741,452	881,063
43	AES 2–3[a]	Qt2	16.35	120	235	115	740,279	881,606
44	AES 7b	Qt5	17.00	125	158	33	739,980	880,972
45	AES 8a	Qt7	17.10	119	137	18	740,163	880,675
46	AES 8a	Qt6	17.90	130	158	28	739,319	880,320
47	AES 7b[a]	Qt5	17.90	126	163	37	739,719	880,076
48	AES 8a	Qt6	18.50	135	159	24	739,121	879,738
49	AES 7b	Qt5	18.50	132	171	39	738,960	879,923
50	AES 8a	Qt7	18.90	132	150	18	738,736	879,597
51	AES 8a	Qt6	19.10	132	157	25	738,631	879,441
52	AES 8a	Qt6	19.60	137	164	27	738,295	879,093
53	AES 8	Qt8	19.70	137	143	6	738,160	879,050
54	AES 7b	Qt5	19.80	140	177	37	738,245	878,859
55	AES 7b	Qt5	20.30	143	180	37	738,060	878,376

(continued)

Id	mapped terrace name[a]	Revised terrace name (this study)	Distance from Mtn. Front (km)	River elev. (masl)[b]	Strath elev. (masl)[b]	Strath height (m)	Easting[c]	Northing[c]
56	AES 7a	Qt4	20.50	149	200	51	737,520	878,438
57	AES 7b	Qt5	20.50	195	235	40	738,306	877,828
58	AES 6	Qt3t	20.60	148	233	85	738,213	877,677
59	AEI; AES 1	Qt1	20.70	150	350	200	737,999	877,695
60	AES 7b	Qt5	20.80	146	181	35	737,555	878,312
61	AES 2–3	Qt2	20.80	150	300	150	737,828	877,786
62	AES 8	Qt8	21.10	148	153	5	737,342	877,905
63	AES 8a	Qt7	21.25	156	175	19	737,184	877,932
64	AES 8a	Qt7	22.20	156	177	21	736,334	877,499
65	AES 7b	Qt5	22.60	163	205	42	736,021	877,213
66	AES 8	Qt8	22.80	165	171	6	735,823	877,277
67	AES 8a	Qt7	23.00	165	185	20	735,471	877,354
68	AES 2–3	Qt2	23.10	165	330	165	735,577	876,710
69	AES 8	Qt8	23.75	175	180	5	734,865	877,040
70	AES 7a	Qt4	23.80	175	230	55	734,726	877,243
71	AES 8a	Qt6	24.00	176	200	24	734,389	877,294
72	AES 8a	Qt6	24.00	176	201	25	734,587	877,102
73	AES 7b	Qt5	24.24	177	220	43	734,481	876,862
74	AES 7a	Qt4	24.39	177	233	56	734,452	876,704
75	AES 8a	Qt6	24.49	178	202	24	733,975	876,711
76	AES 7b	Qt5	24.59	179	217	38	733,887	876,756
77	AES 8a	Qt6	24.89	180	207	27	733,783	876,391
78	AES 6	Qt3	24.99	180	285	105	733,030	876,445
79	AES 2–3	Qt2	24.99	180	360	180	734,162	876,183
80	AES 7b	Qt5	25.09	180	223	43	733,659	876,350
81	AES 8a	Qt6	25.09	180	208	28	733,732	876,290
82	AEI; AES 1	Qt1	25.09	190	410	220	734,872	875,910
83	AEI; AES 1	Qt1	25.19	190	412	222	734,634	875,942
84	AEI; AES 1	Qt1	25.29	190	415	225	734,773	875,828
85	AES 7a	Qt4	25.39	196	250	54	733,317	876,422
86	AES 8a	Qt7	25.89	196	214	18	733,599	875,422
87	AES 8a	Qt6	25.89	196	220	24	733,531	875,453
88	AES 7b	Qt5	25.89	196	235	39	733,404	875,396
89	AES 7a	Qt4	25.89	196	250	54	733,221	875,355
90	AEI; AES 1	Qt1	25.89	196	415	219	734,081	875,249
91	IMO 1–3	Qt0	25.89	196	495	299	734,819	874,962
92	AES 8	Qt8	25.99	197	202	5	733,566	875,360
93	IMO 1–3	Qt0	26.39	200	550	350	735,342	874,254
94	AES 2–3	Qt2	26.45	199	385	186	733,973	874,652
95	AES 8	Qt8	26.49	200	205	5	733,694	874,786
96	AES 6	Qt3	26.49	200	290	90	732,818	875,059
97	AES 8a	Qt7	26.88	205	222	17	733,460	874,425
98	AES 7a	Qt4	26.98	210	260	50	733,168	874,348
99	AES 7b	Qt5	26.98	210	250	40	733,267	874,395
100	AES 7a	Qt4	27.18	211	263	52	733,022	874,091
101	AES 8a	Qt6	27.33	212	240	28	733,280	874,010
102	AES 2–3	Qt2	27.33	212	405	193	732,751	873,905
103	AES 7b	Qt5	27.48	213	255	42	733,462	873,896
104	AEI; AES 1	Qt1	27.48	213	480	267	732,483	873,816
105	AES 7a	Qt4	27.63	213	265	52	733,526	873,735
106	AES 8a	Qt7	27.78	214	228	14	733,348	873,555
107	IMO 1–3	Qt0	28.08	221	649	428	735,334	873,626
108	IMO 1–3	Qt0	28.10	222	625	403	735,513	873,465
109	IMO 1–3	Qt0	28.38	222	575	353	735,208	873,288
110	IMO 1–3	Qt0	28.38	221	625	404	735,338	873,544
111	AES 8a	Qt6	28.43	222	242	20	733,449	872,905
112	AEI; AES 1	Qt1	28.55	222	530	308	734,209	872,921
113	AES 7a	Qt4	28.98	228	280	52	733,401	872,384
114	AES 8	Qt8	29.18	229	237	8	733,584	872,148
115	AES 8a	Qt7	29.28	229	245	16	733,695	872,111
116	AES 2–3	Qt2	29.28	230	345	115	733,351	871,895
117	b3a	Qt6	29.30	229	257	28	733,784	872,094
118	AES 7b	Qt5	29.48	231	270	39	733,954	871,932
119	AES 8a	Qt6	29.78	233	256	23	733,768	871,585
120	IMO 1–3	Qt0	29.88	234	615	381	736,024	871,999
121	AES 2–3	Qt2	29.98	235	425	190	734,403	871,529
122	AES 2–3	Qt2	30.08	234	400	166	734,372	871,444
123	AES 7b	Qt5	30.38	242	273	31	733,694	871,016
124	AEI; AES 1	Qt1	30.48	242	557	315	734,702	870,674
125	AES 8a	Qt7	30.48	243	258	15	734,125	870,881
126	AES 8	Qt8	30.48	242	248	6	734,062	870,932
127	AES 6	Qt3	31.08	252	375	123	733,259	870,930
128	AES 7a	Qt4	31.08	252	285	33	733,520	870,610
129	AES 2–3	Qt2	31.08	251	430	179	733,050	870,964

(continued)

Id	mapped terrace name[a]	Revised terrace name (this study)	Distance from Mtn. Front (km)	River elev. (masl)[b]	Strath elev. (masl)[b]	Strath height (m)	Easting[c]	Northing[c]
130	AEI; AES 1	Qt1	31.18	254	495	241	732,954	870,944
131	AES 7a	Qt4	31.58	257	295	38	733,265	870,235
132	AES 6	Qt3	31.58	257	380	123	733,061	870,353
133	AES 7b	Qt5	32.28	259	290	31	733,224	869,382
134	AES 8a	Qt6	32.55	262	280	18	732,870	869,254
135	AES 8a	Qt7	32.78	265	278	13	732,886	868,960
136	AES 8	Qt8	33.28	270	275	5	732,653	868,539
137	AES 8a	Qt7	33.48	270	280	10	732,340	868,476
138	AES 8a	Qt6	33.53	271	290	19	732,278	868,456
139	AES 7b	Qt5	33.63	272	300	28	732,140	868,450
140	AES 7a	Qt4	33.78	273	310	37	732,030	868,303
141	AES 8a	Qt6	34.30	281	298	17	731,758	867,936
142	AES 7a	Qt4	34.38	282	325	43	731,753	867,790
143	AES 8a	Qt6	35.05	291	312	21	731,075	867,670
144	AES 8	Qt8	35.28	293	300	7	730,844	867,587
145	AES 7a	Qt4	35.50	293	335	42	730,478	867,290
146	AES 7a	Qt4	35.57	294	335	41	730,733	867,797
147	AES 8a	Qt6	35.77	295	318	23	730,551	867,832
148	AES 8a	Qt7	36.17	305	323	18	730,305	868,170
149	AES 8a	Qt6	36.17	310	335	25	730,253	868,213
150	AES 7a	Qt4	36.27	312	365	53	730,156	868,117
151	AES 8a	Qt7	36.47	318	335	17	729,939	868,178
152	AES 8a	Qt6	37.30	332	358	26	729,277	868,239
153	AES 7a	Qt4	37.35	329	375	46	729,122	868,255
154	AEA 8	Qt8	37.45	334	345	11	729,127	868,160
155	AES 8a	Qt6	37.65	336	360	24	728,928	868,115
156	AES 7a	Qt4	37.85	351	405	54	728,719	867,975
157	AES 7a	Qt4	38.10	353	420	67	728,615	867,789
158	AES 8a	Qt7	38.40	359	375	16	728,532	867,433
159	AES 8a	Qt7	38.60	369	387	18	728,500	867,213
160	AES 8	Qt8	39.00	387	397	10	728,119	866,964

[a] Terraces are from Pignone et al. (1994, 2001). Those designated by a superscript (a) are from the Regione Emilia–Romagna Servizio Geologico, Sismico e dei Suoli online Cartografia geologica e dei suoli, available at: http://www.regione.Emilia–Romagna.it/wcm/geologia/canali/cartografia/sito_cartografia/sito_cartografia.htm.
[b] masl = Meters above sea level.
[c] Spatial reference of data. Projection: WGS_1984_Transverse_Mercator; Linear Unit: Meter (1.000000); Angular Unit: Degree (0.017453292519943299); False Easting: 500,000; False Northing: −4,000,000; Central Meridian: 9; Scale Factor: 0.9996; Latitude of Origin: 0.

DR-2. Geographic information for Musone River terrace strath locations.

Id	mapped terrace name[a]	Revised terrace name (this study)	Distance from Mtn. Front (km)	River elev. (masl)[b]	Strath elev. (masl)[b]	Strath height (m)	Easting[c]	Northing[c]
1	3rd-order	Qt4–5	13.194	37	17	−20	378,345	4,812,869
2	4th-order	Qt7	13.194	37	32	−5	378,213	4,812,552
3	3rd-order	Qt4–5	21.994	81.3	71	−10	370,011	4,815,786
4	4th-order	Qt7	21.794	80	80	0	370,103	4,815,588
5	1st-order	Qt2	27.49	111.1	171	60	364,269	4,815,720
6	2nd-order	Qt3	27.49	111.1	136	25	364,415	4,815,455
7	2nd-order	Qt3	28.39	116.8	152	35	363,502	4,814,834
8	3rd-order	Qt4–5	28.39	116.8	137	20	363,584	4,814,411
9	1st-order	Qt2	29.79	124.2	194	70	362,195	4,814,578
10	4th-order	Qt7	29.59	123.3	123	0	362,629	4,813,504
11	3rd-order	Qt4–5	29.89	124.7	152	27	362,376	4,813,146
12	4th-order	Qt7	29.99	124.9	135	10	362,200	4,813,251
13	1st-order	Qt2	31.089	133	223	90	360,586	4,814,188
14	2nd-order	Qt3	31.189	133.6	199	65	360,630	4,813,908
15	4th-order	Qt7	34.789	166.6	179	12	358,217	4,811,095
16	3rd-order	Qt4–5	36.489	183	210	27	356,979	4,809,971
17	3rd-order	Qt4–5	40.589	228.9	235	6	354,039	4,807,050
18	3rd-order	Qt4	42.089	250.9	275	24	352,811	4,806,153
19	3rd-order	Qt5	42.389	256.9	271	14	352,453	4,806,099
20	3rd-order	Qt4–5	53.862	450.4	450	0	349,592	4,795,975
21	2nd-order	Qt3	53.562	440.5	480	40	349,512	4,796,239
22	3rd-order	Qt4–5	55.9	519.5	520	0	347,718	4,795,353
23	3rd-order	Qt4–5	56.446	537.2	537	0	347,179	4,795,257
24	2nd-order	Qt3	40.789	231.8	292	60	354,001	4,806,834

[a] Terrace names are from mapping by Coltorti et al. (1991).
[b] masl = Meters above sea level.
[c] Spatial reference of data. Projection: International_1924_UTM_Zone_33 N; Linear Unit: Meter (1.000000); Angular Unit: Degree (0.017453292519943299); False Easting: 500,000; False Northing: 0; Central Meridian: 15; Scale Factor: 0.9996.; Latitude of Origin: 0; Datum: D_International_1924.9.0.

Nesci, D. Savelli, and L. Wilson were important in formulating our ideas. Comments on an early version by Dave Anastasio and Zicheng Yu and a formal review by an anonymous reader greatly assisted in the presentation of data and clarification of discussion points.

References

Agenzia per la protezione dell'ambiente e per i servizi tecnici, 2007. Carta Geologica d'Italia alla scala 1:100.000. Available from: http://www.apat.gov.it/Media/carta_geologica_italia/default.htm (accessed November 2007).

Alessio, M., Allegri, L., Coltorti, M., Cortesi, C., Deiana, G., Dramis, F., Improta, S., Petrone, V., 1979. Depositi tardo-wurmiani nell' alto bacino dell' Esino (Appenino marchigiano) – Datazione con il C^{14}. Geografia Fisica e Dinamica Quaternaria 2, 203–205.

Amorosi, A., Farina, M., Severi, P., Preti, D., Caporale, L., Di Dio, G., 1996. Genetically related alluvial deposits across active fault zones: an example of alluvial fan-terrace correlation from the upper Quaternary of the southern Po Basin, Italy. Sedimentary Geology 102 (3–4), 275–295.

Amorosi, A., Barbieri, M., Castorina, F., Colalongo, M.L., Pasini, G., Vaiani, S.C., 1998a. Sedimentology, micropalaeontology, and strontium-isotope dating of a lower–middle Pleistocene marine succession (Argille Azzurre) in the Romagna Apennines, Northern Italy. Bulletin of the Geological Society of Italy 117, 789–806.

Amorosi, A., Caporale, L., Cibin, U., Colalongo, M.L., Pasini, G., Ricci Lucchi, F., Severi, P., Vaiani, S.C., 1998b. The Pleistocene littoral deposits (Imola Sands) of the northern Apennines foothills. Giornale di Geologia 60, 83–118.

Amorosi, A., Colalongo, M.L., Fiorini, F., Fusco, F., Pasini, G., Vaiani, S.C., Sarti, G., 2004. Palaeogeographic and palaeoclimatic evolution of the Po Plain from 150-ky core records. Global and Planetary Change 40 (1–2), 55–78.

Antoine, P., Lautridou, J.P., Laurent, M., 2000. Long-term fluvial archives in NW France: response of the Seine and Somme rivers to tectonic movements, climate variations and sea-level changes. Geomorphology 33, 183–207.

Antoine, P., et al., 2007. Pleistocene fluvial terraces from northern France (Seine, Yonne, Somme): synthesis, and new results from interglacial deposits. Quaternary Science Reviews 26 (22–24), 2701.

Antoniazzi, A., Ferrari, M., Peretto, C., 1993. Il giacimento di Ca' Belvedere di Monte Poggiolo del Pleistocene inferiore con industria litica (Forlì). Bullettino di Paletnologia italiana 84, 1–56.

Argnani, A., Barbacini, G., Bernini, M., Camurri, F., Ghielmi, M., Papani, G., Rizzini, F., Rogledi, S., Torelli, L., 2003. Gravity tectonics driven by Quaternary uplift in the Northern Apennines: insights from the La Spezia-Reggio Emilia geo-transect. Quaternary International 101–102, 13–26.

Bartole, R., 1995. The North Tyrrhenian–Northern Apennines post-collisional system: constraints for a geodynamic model. Terra Nova 7, 7–30.

Bartolini, C., 2003. When did the Northern Apennine become a mountain chain? Quaternary International 101–102, 75–80.

Basili, R., Barba, S., 2007. Migration and shortening rates in the northern Apennines, Italy: implications for seismic hazard. Terra Nova 19, 462–468.

Bell, K., Castorina, F., Rosatelli, G., Stoppa, F., Lavecchia, G., Scalera, G., 2006. Plume activity, magmatism, and the geodynamic evolution of the central Mediterranean. Annals of Geophysics 49 (1), 357–371.

Benedetti, L.C., Tapponnier, P., Gaudemer, Y., Manighetti, I., Van der Woerd, J., 2003. Geomorphic evidence for an emergent active thrust along the edge of the Po Plain: the Broni-Stradella fault. Journal of Geophysical Research 108 (B5), 2238, doi:10.1029/2001JB001546.

Bertotti, G., Capozzi, R., Picotti, V., 1997. Extension controls Quaternary tectonics, geomorphology and sedimentation of the N-Apennies foothills and adjacent Po Plain (Italy). Tectonophysics 282 (1–4), 291–301.

Bigi, G., Cosentino, D., Parotto, M., Sartori, R., Scandone, P. (Eds.), 1992. Structural Model of Italy and Gravity Map, 1:500,000. Quaderni de 'La Ricera Scientifica, No. 114, vol. 3 Florence.

Bigi, S., Cantalamessa, G., Centamore, E., Didaskalou, P., Micarelli, A., Nisio, S., Pennesi, T., Potetti, M., 1997. The Periadriatic basin (Marche-Abruzzi sector, Central Italy) during the Plio-Pleistocene. Giornale di Geologia 59 (1–2), 245–259.

Birkeland, P., 1999. Soils and Geomorphology. Oxford University Press, New York, 430 pp.

Blum, M.D., Valastro Jr., S., 1993. Late quaternary sedimentation, lower Colorado river, Gulf Coastal Plain of Texas. Geological Society of America Bulletin 106, 1002–1016.

Boccaletti, M., Elter, P., Guazzone, G., 1971. Plate tectonics model for the development of the Western Alps and the Northern Apennines. Nature 234, 108–111.

Boccaletti, M., Bonini, M., Corti, G., Gasperini, P., Martelli, L., Piccardi, L., Tanini, C., Vannucci, G., 2004. Seismotectonic Map of the Emilia–Romagna Region, 1:250,000. Regione Emilia – Romagna – CNR. SELCA, Firenze.

Bogaart, P.W., Balen, R.T.V., Kasse, C., Vandenberghe, J., 2003a. Process-based modelling of fluvial system response to rapid climate change–I: model formulation and generic applications. Quaternary Science Reviews 22 (20), 2077–2095.

Bogaart, P.W., Balen, R.T.V., Kasse, C., Vandenberghe, J., 2003b. Process-based modelling of fluvial system response to rapid climate change II. Application to the River Maas (The Netherlands) during the last glacial–interglacial transition. Quaternary Science Reviews 22 (20), 2097–2110.

Bonini, M., 2007. Interrelations of mud volcanism, fluid venting, and thrust-anti-cline folding: examples from the external northern Apennines (Emilia–Romagna, Italy). Journal of Geophysical Research 112, B08413, doi:10.1029/2006JB004859.

Borraccini, F., De Donatis, M., Di Bucci, D., Mazzoli, S., Megna, A., Nesci, O., Santini, S., Savelli, D., Tramontana, M., 2004. Quaternary tectonics of the Northern Marche Region, and implications for active deformation in the outer Northern Apennines. Studi Geologici Camerti, Special Issue, 2002 Workshop COAST-ACTION 625, pp. 39–44.

Bridgland, D.R., 2000. River terrace systems in north-west Europe: an archive of environmental change, uplift and early human occupation. Quaternary Science Reviews 19 (13), 1293–1303.

Bridgland, D.R., Westaway, R., 2008. Preservation patterns of Late Cenozoic fluvial deposits and their implications: results from IGCP 449. Quaternary International 189, 5–38.

Brugnara, R., Zannoner, C. (Eds.), 1997. Parco Regionale Fluviale dello Stirone. Giunti, Firenze, 197 pp.

Bucher, W.H., 1932. "Strath" as a geomorphic term. Science 74, 130–131.

Bull, W.B., 1991. Geomorphic Response to Climatic Change. Oxford University Press, New York, 326 pp.

Bull, W.L., Knuepfer, P.L.K., 1987. Adjustments by the Charwell River, New Zealand, to uplift and climatic changes. Geomorphology 1 (1), 15–32.

Burbank, D.W., Anderson, R.S., 2001. Tectonic Geomorphology. Blackwell Science, Malden, MA, 274 pp.

Burbank, D.W., Leland, J., Fielding, E., Anderson, R.S., Brozovic, N., Reid, M.R., Duncan, C., 1996. Bedrock incision, rock uplift and threshold hillslopes in the northwestern Himalayas. Nature 379, 505–510.

Burger, R.L., Fulthorpe, C.S., Austin Jr., J.A., 2001. Late Pleistocene channel incisions in the southern Eel River basin, Northern California; implications for tectonic vs. eustatic influences on shelf sedimentation patterns. Marine Geology 177 (3–4), 317–330.

van den Berg, M.W., van Hoof, T., 2001. The Maas terrace sequence at Maastricht, SE Netherlands: evidence for 200 m of late Neogene and Quaternary surface uplift. In: Maddy, D., Macklin, M.G., Woodward, J.C. (Eds.), River Basin Sediment Systems: Archives of Environmental Change. A.A. Balkema Publishers, Lisse, pp. 45–86.

Calamita, F., Coltorti, M., Pieruccini, P., Pizzi, A., 1999. Evoluzione strutturale e morfogenesi Plio-Quaternaria dell'Appennino Umbro-Marchigiano tra il preappennino umbro e la costa Adriatica. Bulletin of the Geological Society of Italy 118, 125–139.

Calderoni, G., Coltorti, M., Dramis, F., Magnatti, M., Cilla, G., 1991. Sedimentazione fluviale e variazioni climatiche nell' alto bacino del Fiume Esino durante il Pleistocene superiore. In: Fenomeni di Erosione e Alluvionamento Degli Alvei Fluviali. Universita di Ancona, pp. 171–190.

Calderoni, G., Cilla, G., Dramis, F., Farabollini, P., 1996. Dinamica fluviale eolocenica nella media valle del fiume Potenza. Geografia Fisica e Dinamica Quaternaria 19, 19–28.

Carminati, E., Giunchi, C., Argnani, A., Sabadini, R., Fernandez, M., 1999. Plio-Quaternary vertical motion of the Northern Apennines: insights from dynamic modeling. Tectonics 18 (4), 703–718.

Castellarin, A., Eva, C., Giglia, G., Vai, G.B., 1985. Analisi strutturale del Fronte Appenninico Padano. Giornale di Geologia 47, 47–76.

Cavelli, A., 1999. Alcuni esempi di applicazioni GIS alle ricerche topografiche nel territorio di Cingoli (Macerata). Archeologia e Calcolatori 10, 189–205.

Cavinato, G.P., DeCelles, P.G., 1999. Extensional basins in the tectonically bimodal central Apennines fold-thrust belt, Italy: response to corner flow above a subducting slab in retrograde motion. Geology 27 (10), 955–958.

Centamore, E., Pambianchi, G., Deiana, G., Calamita, F., Cello, G., Dramis, F., Gentili, B., Nanni, T., Pambianchi, G., Farabollini, P.M.C., Consoli, M., 1991. Ambiente Fisico Delle Marche: Geologia – Geomorfologia – Idrogeologia. Regione Marche. S.E.L.C.A., Firenze. scala 1:100,000.

Cilla, G., Coltorti, M., Dramis, F., Farabollini, P., Gentili, B., Pambianchi, G., 1996. Fluvial sedimentation during the early Holocene in the Marchean valleys (central Italy). Il Quaternario 9 (2), 459–464.

Coltorti, M., 1996. Geomorphology and Holocene fluvial evolution of the Musone River valley (Marche Region, Italy). In: Nanni, T. (Ed.), The Musone River Basin: Geology, Geomorphology and Hydrogeology. Grafiche Scarponi, Osimo (AN), pp. 217–236.

Coltorti, M., 1997. Human impact in the Holocene fluvial and coastal evolution of the Marche region, Central Italy. CATENA 30, 311–335.

Coltorti, M., Dramis, F., 1995. The chronology of upper Pleistocene stratified slope-waste deposits in Central Italy. Permafrost and Periglacial Processes 6, 235–242.

Coltorti, M., Pieruccini, P., 1997. Middle–upper Pliocene 'compression' and middle Pleistocene 'extension' in the east-Tiber basin: from 'synform' to 'extensional' basins in the Tyrrhenian side of the northern Apennines (central Italy). Il Quaternario 10, 521–528.

Coltorti, M., Pieruccini, P., 1999. A lower Pliocene planation surface across the Italian Peninsula: a key tool in neotectonic studies. Journal of Geodynamics 29, 323–328.

Coltorti, M., Consoli, M., Dramis, F., Gentili, B., Pambianchi, G., 1991. Evoluzione geomorfologica delle piane alluvionali delle Marche centro-meridionali. Geografia Fisica e Dinamica Quaternaria 14 (1), 87–100.

Cordier, S., Harmand, D., Frechen, M., Beiner, M., 2006. Fluvial system response to Middle and Upper Pleistocene climate change in the Meurthe and Moselle valleys (Eastern Paris Basin and Rhenish Massif). Quaternary Science Reviews 13, 573–574.

Cyr, A.J., Granger, D.E., 2008. Dynamic equilibrium among erosion, river incision, and coastal uplift in the northern and central Apennines, Italy. Geology 36 (2), 103–106.

D'Agostino, N., Jackson, J.A., Dramis, F., Funiciello, R., 2001. Interactions between mantle upwelling, drainage evolution and active normal faulting; an example from the Central Apennines (Italy). Geophysical Journal International 147 (2), 475–497.

D'Anastasio, E., De Martini, P.M., Selvaggi, G., Pantosti, D., Marchioni, A., Maseroli, R., 2006. Short-term vertical velocity field in the Apennines (Italy) revealed by geodetic leveling data. Tectonophysics 418 (3–4), 219–234.

Damiani, A.V., Moretti, A., 1968. Segnalazione di un episodio lacustre würmiano nell' alta valle del Chienti (Marche). Bollettino della Societa Geologica Italiana 87, 171–181.

De Feyter, A.J., Koopman, A., Molenaar, A., Van Den Ende, C., 1986. Detachment tectonics and sedimentation, Umbria–Marche Apennines, Italy. Bulletin of the Geological Society of Italy 105, 65–85.

Dethier, D.P., 2001. Pleistocene incision rates in the Western United States calibrated using Lava Creek B Tephra. Geology 29, 783–786.

Di Bucci, D., Mazzoli, S., 2002. Active tectonics of the Northern Apennines and Adria geodynamics: new data and a discussion. Journal of Geodynamics 34 (5), 687–707.

Di Bucci, D., Mazzoli, S., Nesci, O., Savelli, D., Tramontana, M., De Donatis, M., Borraccini, F., 2003. Active deformation in the frontal part of the Northern Apennines: insights from the lower Metauro River basin area (northern Marche, Italy) and adjacent Adriatic off-shore. Journal of Geodynamics 36, 213–238.

Di Dio, G. (Ed.), 1998. Riserve idriche sotterranee della Regione Emilia–Romagna. RER and Eni-AGIP, S.E.L.C.A., Firenze, p. 120.

Elter, P., Giglia, g., Tongiorgi, M., Trevisan, L., 1975. Tensional and compressional areas in the recent (Tortonian to present) evolution of the Northern Apennines. Bollettino di Geofisica Teorica ed Applicata 17, 3–18.

Eppes, M., Bierma, R., Vinson, D., Pazzaglia, F., 2008. A soil chronosequence study of the Reno River Valley, Italy. Geoderma, doi:10.1016/j.geoderma.2008.07.011.

Fairbanks, R.G., Mortlock, R.A., Chiu, T.-C., Cao, L., Kaplan, A., Guilderson, T.P., Fairbanks, T.W., Bloom, A.L., Grootes, P.M., Nadeau, M.-J., 2005. Radiocarbon calibration curve spanning 0 to 50,000 years BP based on paired ^{230}Th/^{234}U/^{238}U and ^{14}C dates on pristine corals. Quaternary Science Reviews 24 (16–17), 1781–1796.

Feroni, A.C., Leoni, L., Martelli, L., Martinelli, P., Ottria, G., Sarti, G., 2001. The Romagna Apennines, Italy: an eroded duplex. Geological Journal 36, 39–54.

Ferranti, L., Antonioli, F., Mauz, B., Amorosi, A., Dai Pra, G., Mastronuzzi, G., Monaco, C., Orru, P., Pappalardo, M., Radtke, U., 2006. Markers of the last interglacial sea-level high stand along the coast of Italy: tectonic implications. Quaternary International 145–146, 30–54.

Finnegan, N.J., Roe, G., Montgomery, D.R., Hallet, B., 2005. Controls on the channel width of rivers: implications for modeling fluvial incision of bedrock. Geology 33, 229–232.

Forlani, E., 1987. Studio idrogeologic della conoide e fattibilita di un canale deviatore della diga sul F. Conca. Cons. Potenziam. Acquedotto, Comuni di Cattolica, Misano, Riccione (dati inediti).

Fuller, I.C., Macklin, M.G., Lewin, J., Passmore, D.G., Wintle, A.G., 1998. River response to high-frequency climate oscillations in southern Europe over the past 200 k.y. Geology 26 (3), 275–278.

García, A.F., 2006. Thresholds of strath genesis deduced from landscape response to stream piracy by Pancho Rico Creek in the Coast Ranges of Central California. American Journal of Science 306, 655–681, doi:10.2475/08.2006.03.

Gardner, T.W., Jorgensen, D.W., Schuman, C., Lemieux, J., 1987. Geomorphic and tectonic process rates: effects of measured time interval. Geology 15, 259–261.

Gasparini, C., Iannaccone, G., Scarpa, R., 1985. Fault-plane solutions and seismicity of the Italian peninsula. Tectonophysics 117 (1–2), 59–78.

Gilbert, G.K., 1877. Report on the Geology of the Henry Mountains. Government Printing Office, Washington, 160 pp.

Grenerczy, G., Sella, G., Stein, S., Kenyeres, A., 2005. Tectonic implications of the GPS velocity field in the northern Adriatic region. Geophysical Research Letters 32 (L16311), doi:10.1029/2005GL022947.

Hancock, G.S., Anderson, R.S., 2002. Numerical modeling of fluvial strath-terrace formation in response to oscillating climate. Geological Society of America Bulletin 114 (9), 1131–1142.

Hancock, G.S., Anderson, R.S., Chadwick, O.A., Finkel, R.C., 1999. Dating fluvial terraces with ^{10}Be and ^{26}Al profiles: application to the Wind River, Wyoming. Geomorphology 27 (1–2), 41–60.

Hardy, S., Poblet, J., 2005. A method for relating fault geometry, slip rate and uplift data above fault-propagation folds. Basin Research 17, 417–424.

Hartshorn, K., Hovius, N., Dade, W.B., Slingerland, R.L., 2002. Climate-driven bedrock incision in an active mountain belt. Science 397, 2036–2038.

Hemming, S.R., 2004. Heinrich events: massive late Pleistocene detritus layers of the North Atlantic and their global climate imprint. Review of Geophysics 42, RG1005, doi:10.1029/2003RG000128.

Kligfield, R., 1979. The Northern Apennines as a collisional orogen. American Journal of Science 279, 676–691.

Knox, J.C., 1975. Concept of the graded stream. In: Melhorn, W.N., Flemal, R.C. (Eds.), Theories of Landform Development, Proceedings of the 6th Geomorphology Symposium, Publications in Geomorphology. State University of New York at Binghamton, Binghamton, pp. 169–198.

Lambeck, K., Antonioli, F., Purcell, A., Silenzi, S., 2004. Sea level change along the Italian coast for the past 10,000 yr. Quaternary Science Reviews 23 (14–15), 1567–1598.

Lavé, J., Avouac, J.P., 2000. Active folding of fluvial terraces across the Siwaliks Hills, Himalayas of central Nepal. Journal of Geophysical Research 105 (B3), 5735–5770.

Lavé, J., Avouac, J.P., 2001. Fluvial incision and tectonic uplift across the Himalayas of central Nepal. Journal of Geophysical Research 106 (B11), 26,561–26,591.

Lavecchia, G., Boncio, P., Creati, N., 2003. A lithospheric-scale seismogenic thrust in central Italy. Journal of Geodynamics 36 (1–2), 79–94.

Lipparini, T., 1939. I terrazi fluviali delle Marche. Giornale di Geologia 13, 5–22.

Lipparini, T., Valletta, M., Perella, G., 1968. Carta Geologica D'Italia: Foglio 100 – Forli, 1:100,000. Servizio Geologico D'Italia, Firenze.

Lisiecki, L.E., Raymo, M.E., 2005. A Pliocene–Pleistocene stack of 57 globally distributed benthic d^{18}O records. Paleoceanography 20, PA1003, doi:10.1029/2004PA001071.

Mackin, J.H., 1948. Concept of the graded river. Geological Society of America Bulletin 59, 463–512.

Malinverno, A., Ryan, W., 1986. Extension in the Tyrrhenian Sea and shortening in the Apennines as a result of arc migration driven by sinking of the lithosphere. Tectonics 5, 227–245.

Mariani, S., Mainiero, M., Barchi, M., van der Borg, K., Vonhof, H., Montanari, A., 2007. Use of speleologic data to evaluate Holocene uplifting and tilting: an example from the Frasassi anticline (northeastern Apennines, Italy). Earth and Planetary Science Letters 257 (1–2), 313„ doi:10.1016/j.epsl.2007.02.045.

Martelli, L., Benini, A., De Nardo, M.T., Severi, P., 2008. Note Illustrative della Carta Geologica D'Italia, Foglio 220, Casalecchio di Reno. Regione Emilia Romagna e APAT, scala 1:50,000. Servicio Geologico, Sismico e dei Suoli, Regione Emilia Romagna, Bologna. 12p. 4.

Mayer, L., Menichetti, M., Nesci, O., Savelli, D., 2003. Morphotectonic approach to the drainage analysis in the North Marche region, central Italy. Quaternary International 101–102, 157–167.

McKenzie, D., 1972. Active tectonics of the Mediterranean region. Geophysical Journal of the Royal Astronomical Society 30, 109–185.

Merritts, D., Vincent, K., 1989. Geomorphic response of coastal streams to low, intermediate, and high rates of uplift, Mendocino triple junction region, northern California. Geological Society of America Bulletin 101, 1373–1388.

Merritts, D., Vincent, K., Wohl, E., 1994. Long river profiles, tectonism, and eustasy: a guide to interpreting fluvial terraces. Journal of Geophysical Research 99 (B7), 14031–14050.

Meyer, G.A., Wells, S.G., Jull, A.J.T., 1995. Fire and alluvial chronology in Yellowstone National Park: climate and intrinsic controls on Holocene geomorphic processes. Geological Society of America Bulletin 107, 1211–1230.

Montgomery, D.R., 2004. Observations on the role of lithology in strath terrace formation and bedrock channel width. American Journal of Science 304, 454–476.

Montone, P., Amato, A., Pondrelli, S., 1999. Active stress map of Italy. Journal of Geophysical Research 104 (B11), 25595–25610.

Montone, P., Mariucci, M.T., 1999. Active stress along the NE external margin of the Apennines: the Ferrara arc, northern Italy. Journal of Geodynamics 28, 251–265.

Montone, P., Mariucci, M.T., Pondrelli, S., Amato, A., 2004. An improved stress map for Italy and surrounding regions (central Mediterranean). Journal of Geophysical Research 109, B10410, doi:10.1029/2003JB002703.

Nanni, T., 1996. Geological characteristics of the basin of river Musone. In: Nanni, T. (Ed.), The Musone River Basin: Geology, Geomorphology and Hydrogeology. Grafiche Scarponi, Osimo (AN), pp. 193–215.

Nanni, T., Coltorti, M., Garzonio, C.A., 1996. Bacino Idrografico del Fiume Musone: Geologia – Geomorfologia – Idrogeologia, 1:50,000. Regione Marche, S.E.L.C.A., Fierenze.

Nesci, O., Savelli, D., 1990. Valley terraces in the Northern Marche Apennines (Central Italy): cyclic deposition and erosion. Giornale di Geologia 52 (1–2), 189–195.

Nesci, O., Savelli, D., Calderoni, G., Elmi, C., Veneri, F., 1995. Le antiche piane di fondovalle nell'Appennino Nord-Marchigiano. In: Castiglioni, G.B., Federici, P.R. (Eds.), Assetto fisico e problemi ambientali delle pianure italiane. Memorie Società Geologica Italiana, pp. 293–312.

Pan, B.T., Burbank, D., Wang, Y.X., Wu, G.J., Li, J.J., Guan, Q.Y., 2003. A 900 ky record of strath terrace formation during glacial-interglacial transitions in northwest China. Geology 31 (11), 957–960.

Patacca, E., Sartori, R., Scandone, P., 1990. Tyrrhenian Basin and Apenninic arcs – kinematic relations since late Tortonian times. Memorie della Societa Geologica Italiana 45, 425–451.

Pauselli, C., Barchi, M.R., Federico, C., Magnani, M.B., Minelli, G., 2006. The crustal structure of the northern Apennines (Central Italy): an insight by the crop03 seismic line. American Journal of Science 306 (6), 428–450.

Pazzaglia, F.J., Gardner, T.W., 1993. Fluvial terraces of the lower Susquehanna River. Geomorphology 8, 83–113.

Pazzaglia, F.J., Brandon, M.T., 2001. A fluvial record of rock uplift and shortening across the Cascadia forearc high. American Journal of Science 301, 385–431.

Pazzaglia, F.J., Gardner, T.W., Merritts, D.J. (Eds.), 1998. Bedrock Fluvial Incision and Longitudinal Profile Development over Geologic Time Scales Determined by Fluvial Terraces. Geophysical Monograph Series, vol. 107. Bedrock Channels: American Geophysical Union, pp. 207–235.

Peola, P., 1940. Il paleolitico nella valle del Musone (Marche). Soc. Sci. Genova, Atti foglio 3, 223–245.

Personius, S.F., 1995. Late Quaternary stream incision and uplift in the forearc of the Cascadia subduction zone, western Oregon. Journal of Geophysical Research 100, 20193–20210.

Piccinini, D., Chiarabba, C., Augliera, P., 2006. Compression along the northern Apennines? Evidence from the Mw 5.3 Monghidoro earthquake. Terra Nova 18 (2), 89–94.

Picotti, V., Pazzaglia, F.J., 2008. A new active tectonic model for the construction of the Northern Apennines mountain front near Bologna (Italy). Journal of Geophysical Research 113, B08412, doi:10.1029/2007JB005307.

Pignone, R., Borsetti, A.M., Negri, A., Farabegoli, A., Benini, A., De Donatis, M., Martelli, L., Pizziolo, M., Severi, P., Angelelli, A., Forni, S., 1994. NonEnCarta geologica dell' Appennino Emiliano-Romagnolo: Foglio 265 – S. Piero in Bagno, 1:50,000. S.E.L.C.A., Fierenze.

Pignone, R., Cremonini, G., Antolini, P., Pialli, G., Ricci Lucchi, F., Borsetti, A.M., 2001. Carta geologica regionale: Rocca San Casciano – 254 SE, 1:25,000. Regione Emilia–Romagna, Bologna.

Pini, G.A., 1999. Tectonosomes and olistostromes in the argille scagliose of the Northern Apennines, Italy. In: Geological Society of America, Special Paper, vol. 335, 70 pp.

Pondrelli, S., Salimbeni, S., Ekstrom, G., Morelli, A., Gasperini, P., Vannucci, G., 2006. The Italian CMT dataset from 1977 to the present. Physics of the Earth and Planetary Interiors 159 (3–4), 286–303.

Ramsay, B., 2005. OxCal Version 3.10. downloaded in November, 2005. University of Oxford, Oxford, UK. Available from:. http://c14.arch.ox.ac.uk/oc_3_10r.exe.

Reutter, K.J., 1981. A trench-forearc model for the Northern Apennines. In: Wezel, F.C. (Ed.), Sedimentary Basins of Mediterranean Margins. C.N.R. Italian Project of Oceanography, Tecnoprint, Bologna, pp. 433–443.

Ricci Lucchi, F., 1986. The Oligocene to recent foreland basins of the northern Apennines. In: Allen, P.A., Homewood, P. (Eds.), Foreland Basins: Special Publication of the International Association of Sedimentologists. Blackwell Scientific Publishing, Oxford, England, pp. 105–139.

Royden, L.H., 1993. Evolution of retreating subduction boundaries formed during continental collision. Tectonics 12 (3), 629–638.

Santisteban, J.I., Schulte, L., 2007. Fluvial networks of the Iberian Peninsula: a chronological framework. Quaternary Science Reviews 26 (22–24), 2738–2757.

Savelli, D., Nesci, O., Mengoni, S., 1996. From alluvial fans to intravalive floodplain: a case study from the piedmont terrace alluvium of the upper Musone River basin (Marche Apennines). Giornale di Geologia 56, 27–42.

Schumm, S.A., 1969. River metamorphosis. Proceedings of the American Society of Civil Engineers. Journal of the Hydraulics Division 95, 255–273.

Schumm, S.A., Mosley, M.P., Weaver, W.E., 1987. Experimental Fluvial Geomorphology. Wiley Interscience, New York, 413 pp.

Scrocca, D., 2006. Thrust front segmentation induced by differential slab retreat in the Apennines (Italy). Terra Nova 18 (2), 154–161.

Seidl, M.A., Dietrich, W.E., 1992. The problem of channel erosion into bedrock. In: Schmidt, K.H., de Ploey, J. (Eds.), Functional Geomorphology: Catena, Suppl. 23, pp. 101–124.

Selvaggi, G., Ferulano, F., Di Bona, M., Frepoli, A., Azzara, R., Basili, A., Chiarabba, C., Ciaccio, M.G., Di Luccio, F., Lucente, F.P., Margheriti, L., Nostro, C., 2001. The Mw 5.4 Reggio Emilia 1996 earthquake: active compressional tectonics in the Po Plain, Italy. Geophysical Journal International 144 (1), 1–13.

Serpelloni, E., Anzidei, M., Baldi, P., Casula, G., Galvani, A., 2005. Crustal velocity and strain-rate fields in Italy and surrounding regions: new results from the analysis of permanent and non-permanent GPS networks. Geophysical Journal International 161 (3), 861–880.

Simoni, A., Elmi, C., Picotti, V., 2003. Late Quaternary uplift and valley evolution in the Northern Apennines: lamone catchment. Quaternary International 101–102, 253–276.

Sklar, L., Dietrich, W.E., 1998. River longitudinal profiles and bedrock incision models: stream power and the influence of sediment supply. In: Wohl, E., Tinkler, K. (Eds.), Rivers over Rock: Fluvial Processes in Bedrock Channels. American Geophysical Union Geophysical Monograph Series, pp. 237–260.

Stramondo, S., Saroli, M., Tolomei, C., Moro, M., Doumaz, F., Pesci, A., Loddo, F., Baldi, P., Boschi, E., 2007. Surface movements in Bologna (Po Plain – Italy) detected by multitemporal DInSAR. Remote Sensing of Environment 110 (3), 304–316.

Sugai, T., 1993. River terrace development by concurrent fluvial processes adn climatic changes. Geomorphology 6, 243–252.

Taddeucci, A., Tuccimei, P., Voltaggio, M., 1992. Studio geocronologico del complesso carsico "Grotta del Fiume-Grotta Grande del Vento" (Gola di Frasassi, AN) e implicazioni paleoambientali. Il Quaternario 5, 213–222.

Thackray, G.D., 1998. Convergent-margin deformation of Pleistocene strata on the Olympic coast of Washington, USA. In: Stewart, I.S., Vita-Finzi, C. (Eds.), Coastal Tectonics. Geological Society [of London], Special Publication, vol. 146, pp. 199–211. London.

Tornqvist, T.E., Wallinga, J., Murray, A.S., de Wolf, H., Cleveringa, P., de Gans, W., Cloetingh, S.A.P.L. (Eds.), 2001. Response of the Rhine-Meuse System (west-central Netherlands) to the Last Quaternary Glacio-Eustatic Cycles; a First Assessment. Elsevier, Amsterdam, Netherlands, pp. 89–111.

Tucker, G.E., Slingerland, R., 1997. Drainage basin response to climate change. Water Resources Research 33 (8), 2031–2047.

Vannoli, P., Basili, R., Valensise, G., 2004. New geomorphic evidence for anticlinal growth driven by blind-thrust faulting along the northern Marche coastal belt (central Italy). Journal of Seismology 8, 297–312.

Veldkamp, A., van Dijke, J.J., 2000. Simulating internal and external controls on fluvial terrace stratigraphy: a qualitative comparison with the Maas record. Geomorphology 33 (3–4), 225–236.

Villa, G.M., 1942. Nuove ricerche sui terrazzi fluviali delle Marche. Giornale di Geologia 16, 5–75.

Watts, W.A., Allen, J.R.M., Huntley, B., 2000. Palaeoecology of three interstadial events during oxygen-isotope stages 3 and 4: a lacustrine record from Lago Grande di Monticchio, southern Italy. Palaeogeography Palaeoclimatology Palaeoecology 155 (1–2), 83–93.

Wegmann, K.W., 1999. Late Quaternary Fluvial and Tectonic Evolution of the Clearwater River Basin, Western Olympic Mountains, Washington State. M.S. thesis. Albuquerque, University of New Mexico, 217 pp.

Wegmann, K.W., Pazzaglia, F.J., 2002. Holocene strath terraces, climate change, and active tectonics; the Clearwater River basin, Olympic Peninsula, Washington State. Geological Society of America Bulletin 114 (6), 731–744.

Wegmann, K.W., 2008. Tectonic Geomorphology above Mediterranean Subduction Zones: Northeastern Apennines of Italy and Crete, Greece. Ph.D. thesis. Lehigh University, Bethlehem, PA, 169 pp.

Weldon, R.J., 1986. Late Cenozoic Geology of Cajon Pass; Implications for Tectonics and Sedimentation Along the San Andreas fault. Ph.D. thesis. Pasadena, California Institute of Technology, 400 pp.

Westaway, R., 2001. Flow in the lower continental crust as a mechanism for the Quaternary uplift of the Rhenish Massif, north-west Europe. In: Maddy, D., Macklin, M.G., Woodward, J.C. (Eds.), River Basin Sediment Systems: Archives of Environmental Change. A.A. Balkema Publishers, Lisse, pp. 87–167.

Wezel, F.C., 1982. The Tyrrhenian Sea: a rifted krikogenic-swell basin. Memorie della Societa Geologica Italiana 24, 531–568.

Woolfe, K.J., Larcombe, P., Naish, T., Purdon, R.G., 1998. Lowstand rivers need not incise the shelf; an example from the Great Barrier Reef, Australia, with implications for sequence stratigraphic models. Geology 26 (1), 75–78.

Wortel, M.J.R., Spakman, W., 2000. Subduction and slab detachment in the Mediterranean-Carpathian region. Science 290, 1910–1917.

Zaprowski, B.J., Evenson, E.B., Pazzaglia, F.J., Epstein, J., 2001. Knickzone propagation in the Black Hills and northern High Plains; a different perspective on the late Cenozoic exhumation of the Laramide Rocky Mountains. Geology 29 (6), 547–550.

Zattin, M., Landuzzi, A., Picotti, V., Zuffa, G.G., 2000. Discriminating between tectonic and sedimentary burial in a foredeep succession, Northern Apennines. Journal of the Geological Society 157, 629–633.

Zattin, M., Picotti, V., Zuffa, G.G., 2002. Fission-track reconstruction of the front of the northern Apennine thrust wedge and overlying Ligurian Unit. American Journal of Science 302 (4), 346–379.